Physica **104A** (1980) 509–547 © *North-Holland Publishing Co.*

THE BROADENING AND SHIFT OF THE ROTATIONAL RAMAN LINES FOR HYDROGEN ISOTOPES AT LOW TEMPERATURES

K.D. VAN DEN HOUT†, P.W. HERMANS, E. MAZUR and H.F.P. KNAAP

Huygens Laboratorium der Rijksuniversiteit, Leiden, The Netherlands

Received 27 June 1980

Collisional broadening of rotational Raman lines has been investigated for the gases nH_2, nD_2 and HD between 20 and 300 K. For H_2 and D_2 the dependence of the linewidth on ortho–para composition has been investigated. For a number of systems the pressure shift of the Raman lines has also been determined. The experimental results are compared with theory.

1. Introduction

For many years the rotational Raman lines have been an abundant source of information on the molecular properties of matter. The most intensively investigated aspect, the differences between the frequencies of the Raman lines and the frequency of the exciting light, is commonly used for the determination of molecular structure parameters. Another important feature, the shape of the line, is the main subject of this paper. The spectral line shape is dependent on the density of the scattering medium and reflects the time evolution of the molecular translational and rotational states. Because these states are perturbed by molecular interactions, the line shape can be used to extract information about the intermolecular collision processes[1–3]).

In a rotational Raman light scattering process, energy is exchanged between a photon and a molecule. Such a molecule, designated here as radiating molecule or radiator, undergoes an internal energy transition and the light, scattered out of a usually monochromatic beam of light, is altered in frequency. The selection rule for such a transition in linear molecules is $J_f - J_i = \pm 2$, where J_f and J_i indicate the final and initial rotational states of the spectroscopic transition. The lines appear in the spectrum of the scattered light as two series of equidistant lines at either side of the exciting frequency. In this study the lines corresponding to the transition $J_f - J_i = +2$, the Stokes lines, are investigated. These are usually denoted by $S_0(J_i)$, where the subscript 0 indicates that only the lowest vibrational level is involved. The anti-Stokes lines ($J_f - J_i = -2$) are theoretically known to behave similarly to the Stokes lines[4]).

† Present address: Research Institute for Environmental Hygiene-TNO, Delft, The Netherlands.

In the absence of collisions, the spectral line shape is determined by natural broadening and Doppler broadening. Since the natural linewidth is very small, the spectral line shape of a Raman line of a gas in the low density limit reflects the velocity distribution of the scattering molecules. When the density is slightly increased, the molecular translational motion is no longer free, but becomes affected by intermolecular collisions and the linewidth is thereby related to the translational diffusional motion of the radiating molecules. The rotational motion of the molecules is also influenced by collisions and, since the amplitude, frequency and phase of the scattered light wave are dependent on the internal molecular state, such collisions can, in general, disturb the radiation process and thus give rise to collisional line broadening and a shift of the central line frequency (collisional line shift). At higher densities, where the mean free path of the molecules becomes considerably smaller than the wavelength of the light, the collisional broadening dominates over the broadening that is due to the diffusional motion. The spectral line shape can then be described by a Lorentzian profile[5-7]):

$$I(\nu) = \frac{I_0}{\pi} \frac{\Delta\nu_{1/2}(\rho)}{(\nu - \nu_R(\rho))^2 + \Delta\nu_{1/2}(\rho)^2}. \tag{1}$$

$I(\nu)$ is the intensity at frequency ν, I_0 is the integrated line intensity and $\Delta\nu_{1/2}(\rho)$ is the halfwidth*, which depends on the density ρ. $\nu_R(\rho)$, the central frequency of the Raman line at density ρ, is, for Stokes rotational Raman lines, given by

$$\nu_R(\rho) = \nu_0 - h^{-1}(E_{J_f} - E_{J_i}) + \Delta\nu_S(\rho), \tag{2}$$

where ν_0 is the frequency of the exciting light and $h^{-1}(E_{J_f} - E_{J_i})$ is the Raman frequency displacement corresponding to the energy difference between the unperturbed final and initial levels of the spectroscopic transition. $\Delta\nu_S(\rho)$ is the (density dependent) collisional line shift, which is negative when the line shifts away from ν_0. When the broadening due to the translational motion can be neglected, $\Delta\nu_{1/2}(\rho)$ and $\Delta\nu_S(\rho)$ are proportional to the density, provided that the density is not so high that ternary or higher order collisions occur at an appreciable rate. We shall restrict ourselves to that region of the binary collision regime where the collisional broadening is predominant.

Usually, the line broadening process is governed by many different collision processes, and consequently a detailed interpretation is in general difficult. In this respect, gases of hydrogen isotopes where only a small number of internal states are populated are very interesting. Especially at low temperatures, the number of collisional transitions that are possible is very small. Furthermore, several significantly different, yet closely related systems (oH_2, pH_2, oD_2, pD_2, HD) are available for investigation.

* The halfwidth indicates half the (full) width at half height.

Before proceeding with a description of the experiments on the hydrogen isotopes, it is useful to review a few pertinent characteristics of these molecules. The most obvious distinction between the isotopes is the difference in molecular mass (and therefore in moment of inertia), which is reflected in the energy separation of the rotational levels. In fig. 1 a diagram of the rotational energies is presented for H_2, D_2 and HD. For the homonuclear molecules H_2 and D_2 the symmetry properties of the nuclear spin statistics forbid transitions $\Delta J = \pm 1$. The energy involved in rotational transitions is usually rather large as compared with the thermal energy: $\Delta E_{rot} \geqslant k_B T$.

The fact that transitions between ortho and para states are not allowed has important consequences for the population of the rotational states of H_2 and D_2 at low temperatures (fig. 2). The lowest rotational level in the "odd" modifications oH_2 and pD_2 corresponds to $J = 1$ and hence internal rotational energy is present even at the low temperature limit.

Extensive measurements of the broadening of the rotational Raman lines of hydrogen isotopes at room temperature have been performed by Keijser et al.[7]). Their results for H_2 as a function of the ortho–para composition indicated that an important contribution to the linewidth is due to so-called resonance collisions. These are collisions in which the rotational energy changes occurring in the two collision partners exactly compensate each other.

In this paper an experimental investigation of the collisional broadening of the rotational Raman lines of nH_2, nD_2 and HD and the mixtures 90% pH_2–10% oH_2 and 23% oD_2–77% pD_2 between 25 K and 300 K is reported. The scattering gas densities were typically 1000–5000 mol/m^3 (about 20–100 amagat). Although the

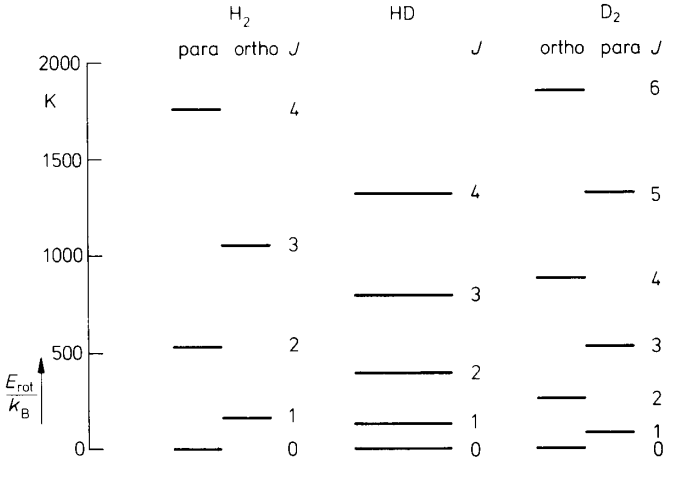

Fig. 1. Diagram for the rotational energy levels of H_2, D_2 and HD.

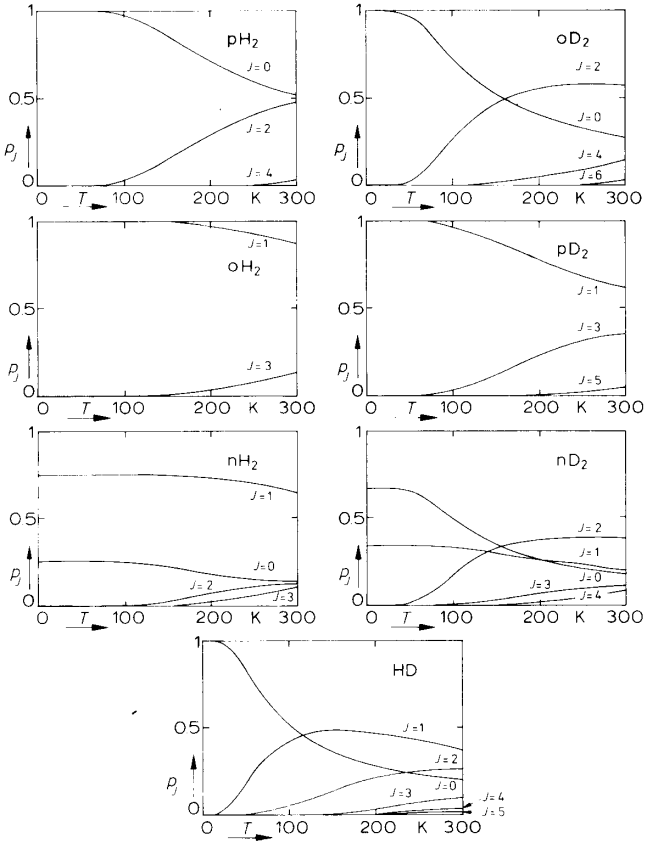

Fig. 2. The fractional population of the rotational energy levels as a function of temperature for the different modifications of H_2 and D_2 and for HD.

main purpose was to study the linewidths, the collisional line shifts were also determined in the course of the measurements.

In the second part of the paper the experimental setup and the numerical analysis of the spectra is discussed. Next the experimental results are presented and, finally, an interpretation of the observed behavior of the line broadening effect with respect to temperature, ortho–para composition and isotopic species is proposed.

2. Experimental

2.1. *Apparatus*

The apparatus used to measure the broadening and shift of the rotational Raman lines at low temperatures, was very similar to the one used by Keijser et

al. for the investigation of the depolarized Rayleigh line and the rotational Raman lines at room temperature[7,8]). For the present measurements a new type of scattering cell was devised which could be used at temperatures between 5 K and 300 K. It was mounted in an optical cryostat. A schematic diagram of the optics is given in fig. 3. A horizontal beam of light from an Ar ion laser was focussed into the scattering cell. The laserlight was horizontally polarized, i.e., with the electric vector in the horizontal plane. The light scattered at right angles to the laser beam was collected and passed through a polarizer which transmitted only the horizontally polarized component. For the spectroscopic analysis a Fabry–Pérot interferometer was used in combination with a small monochromator. Because the monochromator was set to transmit only the particular Raman line under investigation, the interferometer could then be used to measure the spectral line with high resolution. The transmitted light was detected by a low noise photomultiplier together with photon counting equipment.

In the following the various parts of the setup will be discussed in more detail.

Laser. A Spectra Physics model 165 single mode Ar ion laser, operating at 514.5 nm, was used as the light source. The output power (about 1 W) varied less than 1% during one measurement.

Scattering cell and cryostat. The scattering gas was contained in a brass cell designed for pressures up to 75 atm. In fig. 4 a schematic picture is given of the cell together with the cryostat. A number of diaphragms (not shown in the picture) were placed inside the cell to suppress the intense stray light scattered from the laser beam by the cell windows.

A small white screen could be moved into the center of the cell by means of a

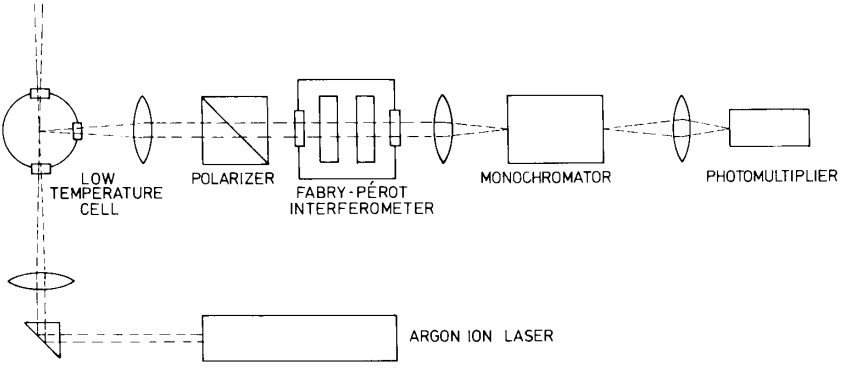

Fig. 3. Schematic diagram of the experimental setup.

small magnet (not shown in fig. 4). It was used for alignment purposes and for the determination of the instrumental contribution to the spectral linewidth.

The cell was in direct contact with an Oxford Instrument CF 100 Continuous Flow Cryostat. Cooling was achieved by pumping a coolant (liquid N_2 or He) through a heat exchanger. Fine regulation of the temperature was obtained with an electrical heater. The stability over one measurement (with a typical duration of several hours) was 0.1 K and the short term stability appreciably better.

A platinum resistance thermometer was attached to the cell to measure the temperature of the scattering gas.

Interferometer. The Fabry–Pérot interferometer consisted of two flat mirrors, contained in a temperature stabilized pressure chamber. The mirrors were polished to a flatness of $\lambda/300$ and coated for a reflectance of 97% in the region between 500 and 550 nm. The free spectral range (i.e., the frequency separation of the interferometer orders) was chosen to be 38.95 GHz or 75.56 GHz,

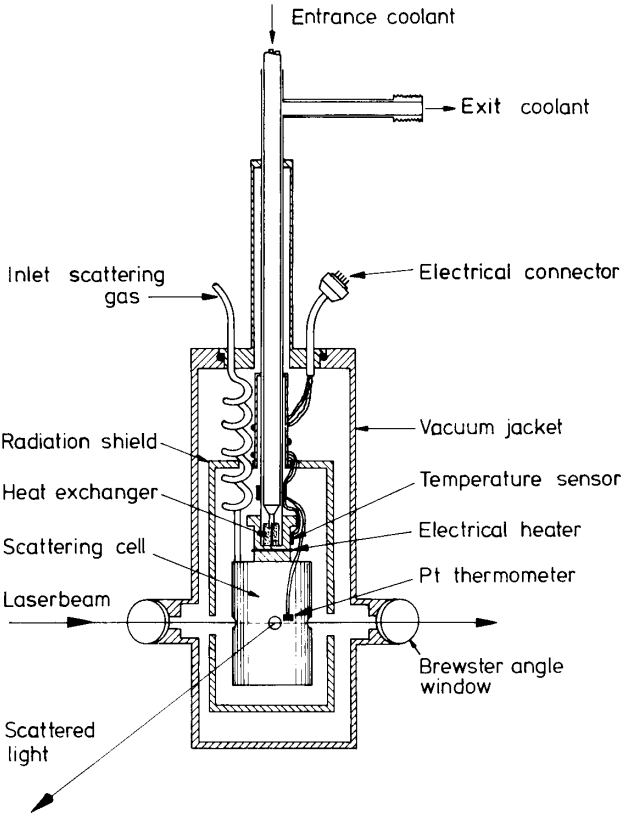

Fig. 4. Schematic diagram of the optical cryostat.

depending on the width of the measured line. The optical path length of the beam crossing the interferometer was varied by changing stepwise the pressure of the gas in the chamber. After each step the detected intensity was measured at constant pressure. In this way a highly linear scanning could be achieved. The overall finesse was typically 35.

Monochromator and polarizer. A Jarrell Ash 25 cm monochromator was used to select a particular Raman line from the spectrum. For almost all measurements the full width of the transmission profile of the monochromator was 0.8 nm (corresponding to 900 GHz); in a few cases 0.4 nm.

Special care had to be taken to avoid spurious effects in the observed spectrum due to the very strong, polarized Rayleigh–Brillouin triplet. Because the detected intensity of the Raman lines depends only weakly on the polarization of the exciting light[9]), a geometrical arrangement of the setup was chosen so as to suppress the polarized part of the spectrum: with the laser beam horizontally polarized, the light scattered at right angles in the horizontal plane was detected. However, as a result of stress birefringence in the cell windows which occurred at low temperatures, a strong, vertically polarized contribution from the Rayleigh–Brillouin triplet was observed in the scattered light. Since the straylight rejection of the monochromator was not sufficient to reject this spurious component, a Glan–Thompson polarizer was inserted in front of the interferometer, which transmitted only the horizontally polarized part of the scattered light. At the densities studied, the Raman spectrum is virtually independent of the polarization of the exciting light.

Detection system. The light, detected by a thermoelectrically cooled ITT FW 130 photomultiplier, was analyzed by a photon counting system and the detected intensity at each spectral point was punched on paper tape. The intensities measured at the top of the Raman lines were between 5 and 1000 counts per second. The dark noise level was about one count every two seconds. Because of the low light levels, the time required to measure the spectrum of a Raman line was rather long, usually 2–12 hours.

2.2. *Gas handling procedure*

nH_2 (containing 25% pH_2) and nD_2 (67% oD_2) were obtained commercially. The purity of nH_2 was better than 99.9%, of nD_2 better than 99.6%. HD was prepared by the action of $LiAlH_4$ on D_2O[10]). After purification and fractional distillation, the main contaminants were D_2 (1.2%) and H_2 (0.2%). pH_2 was prepared by catalytic conversion of nH_2 into equilibrium H_2 on iron oxide at 20 K. In the experiments, a mixture of 90% pH_2 was investigated (rather than

nearly pure pH_2), because at this concentration the Raman lines involving odd J levels were sufficiently intense to permit accurate measurements. For D_2 one needed both nD_2, which has a high oD_2 concentration (67%), and a mixture with a low oD_2 content. Such a mixture was prepared using a method based on the preferential adsorption of pD_2 on Al_2O_3 at 20 K [11]).

The rate of conversion to the equilibrium ortho–para composition was monitored between successive linewidth measurements. This was accomplished by allowing the scattered light beam to bypass the interferometer and then scanning the rotational Raman spectrum with the monochromator. From the observed intensities of the Raman lines the populations of the rotational states were calculated. It was found that the change in composition over one measurement was usually smaller than one percent. For a few of the measurements of longer duration, a small correction to the linewidth was applied. For the measurements with nH_2 and nD_2, a fresh sample of the gas was introduced into the cell at the beginning of each measurement. For the other ortho–para mixtures, the amounts available were not large enough for such a procedure to be followed. In these cases, therefore, a single gas sample was used for several measurements.

2.3. *Numerical analysis of the spectra*

A typical Raman line spectrum obtained in one measurement is given in fig. 5. The two peaks correspond to consecutive orders of the interferometer. The spectrum was always measured over two such orders.

2.3.1. *Collisional line broadening*

Photomultiplier dark noise. The photomultiplier dark noise level was determined frequently between the experiments. It was found to be very stable and the measured spectra were corrected by subtracting a constant level.

Instrumental contribution. The observed linewidth contained an instrumental

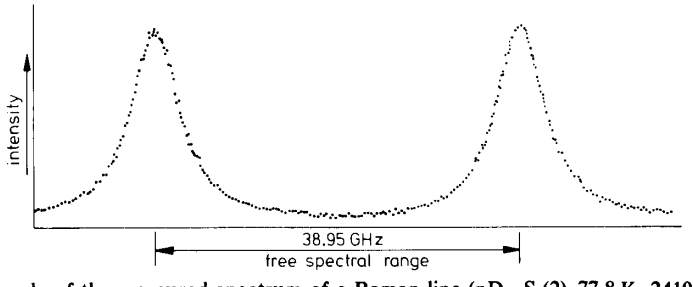

Fig. 5. Example of the measured spectrum of a Raman line (nD_2, $S_0(2)$, 77.8 K, 2410 mol/m^3).

contribution which was almost entirely due to the finite resolution of the interferometer. For the determination of the instrumental profile, the white screen inside the scattering cell was brought into the laser beam. As the diffuse scattering from this screen did not appreciably broaden the laser line, the spectrum of this light corresponds to the instrumental profile. In fig. 6 an example of the instrumental profile is shown. In principle, the instrumental profile depends on the frequency of the scattered light due to dispersion in the lens behind the interferometer, the frequency dependence of the reflection coefficient of the interferometer mirrors, etc. The associated error is estimated to be negligibly small. The halfwidth of the instrumental line was usually around 0.5 GHz and constituted in many cases a fairly large part of the total Raman linewidth. It was therefore necessary that the correction for this broadening be executed very carefully. During a set of experiments, the instrumental profile was always determined several times and it was usually found to be very constant.

Distortion of the instrumental profile, because of the drift of the laser frequency, was small. Laser mode hops, giving rise to a sudden frequency change of 150 MHz, could occasionally affect a measured peak. The associated error is, however, even for the smallest broadening coefficients, estimated to be not larger than 1%, since in all cases at least four peaks were used to obtain one single broadening coefficient.

A Fourier transform technique was employed to remove the instrumental contribution from the observed Raman spectrum $S(\nu)$, which is the convolution of the true Raman line profile $R(\nu)$ and the instrumental profile $O(\nu)$[7,12]:

$$S(\nu) = \int_{-\infty}^{\infty} R(\nu')O(\nu - \nu')\,\mathrm{d}\nu'. \tag{3}$$

$S(\nu)$ and $O(\nu)$ are periodic functions with periods equal to the free spectral range. A simple relation exists between the Fourier transforms of the functions

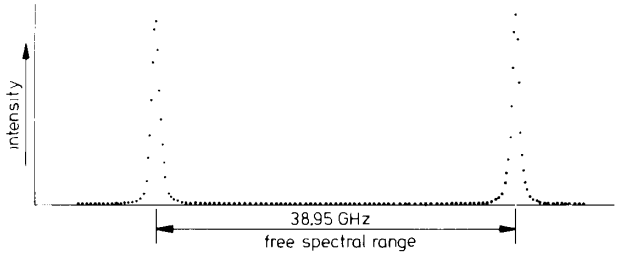

Fig. 6. Example of the measured instrumental profile.

in eq. (3):

$$F_S(t) = F_R(t)F_O(t). \tag{4}$$

Because of the periodicity of the spectral functions $S(\nu)$ and $O(\nu)$, an interval of one free spectral range is sufficient to calculate the Fourier transforms. In the analysis each of the two peaks of one measurement was separately transformed, taking the center frequency of the peak as the zero frequency. The instrumental contribution could then be removed by simple division: $F_R(t) = F_S(t)/F_O(t)$. The results obtained for the two peaks were averaged.

Wing suppression. The wings of the broadest HD Raman lines were partially suppressed by the monochromator. Since the intensity variation of the suppressed part was very small in a free spectral range of the interferometer, a correction to $F_R(t)$ was applied corresponding to the addition of a constant background to the spectrum. The magnitude of this correction was at most 2% of the integrated intensity of the Raman line.

Diffusional contribution. The linewidths obtained from the Fourier transform $F_R(t)$ represent the actual broadening of the rotational Raman lines as determined by the molecular dynamics of the scattering gas. The broadening mechanisms are, apart from the negligibly small natural broadening, the collisional broadening due to perturbations of the internal molecular motion, and the diffusional broadening associated with the translational motion of the molecules. At densities high enough that $kl \ll 1$, where k is the magnitude of the difference between the wave vectors of the incident and of the scattered light, and l is the mean free path of the molecules, the line shape is Lorentzian[5,13]). The halfwidth is then given by:

$$\Delta\nu_{1/2}^{\text{total}} = \Delta\nu_{1/2}^{\text{diff}} + \Delta\nu_{1/2}^{\text{coll}} = \frac{k^2 D_R}{2\pi} + B\rho \tag{5}$$

with

$$D_R \propto 1/\rho. \tag{6}$$

D_R is a diffusion constant (the dependence on the density ρ is explicitly shown), and B is the collisional broadening coefficient.

A correction for the diffusional contribution was applied, using a value for the diffusional constant obtained from literature. For H_2 the self-diffusion constant D was taken as measured at various temperatures by Harteck and Schmidt[14]), Lipsicas[15]) and Hartland[16]). At temperatures where D has not been measured, an interpolated value was used. For HD and D_2 the diffusion constant was

determined from the H_2 data, employing the approximate relation for isotopes:

$$D \propto m^{-1/2}. \tag{7}$$

It is known from experiments performed at room temperature[17,18]), that, for the $S_0(1)$ line of nH_2, the value of D_R is some 20% higher than D. In the density range of our measurements such a difference is, however, too small to affect the line broadening coefficients appreciably (less than 1%).

2.3.2. *Collisional line shift*

The measured spectra yield information not only about the broadening of the Raman lines, but can be used to determine the collisional line shifts as well. In general, the central frequency of the line changes slightly as a function of the scattering gas density. Hence the peak appears in the recorded spectrum at a slightly different pressure of the interferometer scanning gas. The scanning gas pressure at the center of each measured peak was carefully determined. A change of this pressure with density of the scattering gas was then converted into a change of the central frequency of the line. Because the collisional line shift is, in the binary collision regime, linear in the scattering gas density, the line shift coefficient can be determined from two measurements at different densities.

Although accurate measurements of the collisional line shift by such means are possible in principle, the actual experimental conditions imposed rather severe limitations on the reliability of the results. It is instructive to compare the determination of the line shift with that of the line broadening. First, in the case of collisional broadening, corrections can be made for all additional broadening effects. Consequently, a single measurement is, in principle, sufficient to determine a broadening coefficient. In the case of collisional line shift, however, one needs at least two measurements at different densities of the scattering gas for a determination of the collisional line shift. Secondly, the time between two measurements of a Raman line at different scattering gas densities was of the order of a day. Consequently, the long term alignment drifts of the optical system affected the line shift measurements severely. Usually this situation could be improved by taking advantage of the relation between the position of the spectral lines. In a number of cases, where the collisional broadening coefficient has been measured, the corresponding collisional shift coefficients could not be determined because the optics had been realigned between the measurements.

The reliability of the line shift coefficients was checked in a series of measurements of the depolarized Rayleigh line. The shift of this line is theoretically known to vanish; experimentally the shift was found to be zero: 0 ± 0.05 MHz m^3/mol for nH_2 (cf. 1 MHz m^3/mol for a typical Raman line shift).

It should be mentioned that the collisional line shift can be measured with

much greater accuracy if one measures only the part of the spectrum near the center of a Raman line. Then, a series of measurements at different scattering gas densities can be executed within a short time. In a few cases, such a precise determination of the line shift coefficient was accomplished. Good agreement with the value obtained in the usual way was found.

3. Results

3.1. *Collisional line broadening*

The number of lines that can be investigated decreases at lower temperatures, as the number of populated rotational states becomes smaller. In our experimental arrangement, a reliable determination of the linewidth was possible when the relative population of the initial state associated with the line was not smaller than about 0.2%. Only the $S_0(0)$ and $S_0(1)$ lines could be studied over the entire temperature range. The gas temperature could not be chosen arbitrarily low, since accurate results could be obtained only when the density range of the measurements extended up to at least 1200 mol/m^3. The requirement that the density should be somewhat lower than the vapor density made measurements below 25 K unfeasible.

In figs. 7, 8 and 9 some typical examples of the Fourier transforms of the line spectra $F_R(t)$ are plotted on a semi-logarithmical scale as a function of time. $F_R(0)$ is normalized to unity. As should be expected, an exponentially

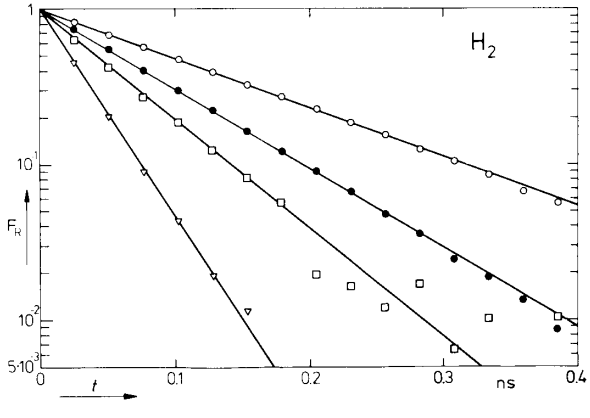

Fig. 7. Typical examples of the Fourier transform F_R as a function of time for H_2: ○ 93% pH_2 + 7% oH_2, $S_0(1)$, 77.8 K, 3110 mol/m^3; ● nH_2, $S_0(0)$, 52.7 K, 2490 mol/m^3; □ nH_2, $S_0(3)$,137 K, 3430 mol/m^3; ▽ nH_2, $S_0(1)$, 35.0 K, 3470 mol/m^3.

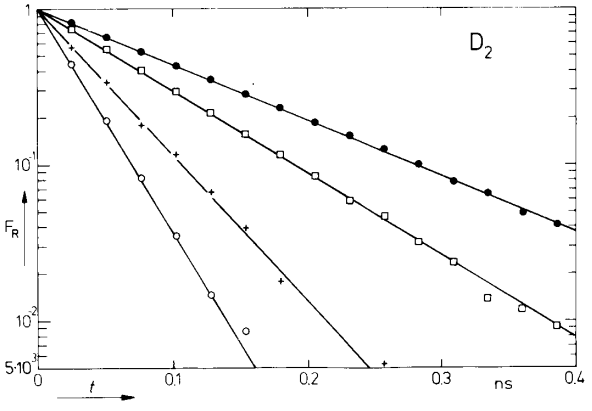

Fig. 8. Typical examples of the Fourier transform F_R as a function of time for D_2: ● 23% oD_2 + 77% pD_2, $S_0(0)$, 28.3 K, 687 mol/m^3; □ nD_2, $S_0(3)$, 148.5 K, 2250 mol/m^3; + nD_2, $S_0(2)$, 42.9 K, 2200 mol/m^3; ○ nD_2, $S_0(1)$, 77.8 K, 4830 mol/m^3.

decaying function was found in all cases:

$$F_R(t) = e^{-t/\tau}. \tag{8}$$

This corresponds to a Lorentzian lineshape in the frequency domain:

$$\frac{1}{2\pi\tau} = \Delta\nu_{1/2}, \tag{9}$$

where $\Delta\nu_{1/2}$ is the collisional halfwidth of the rotational Raman line.

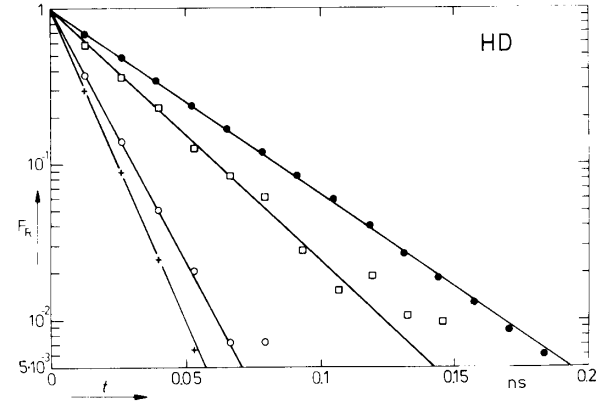

Fig. 9. Typical examples of the Fourier transform F_R as a function of time for HD: ● $S_0(0)$, 27.0 K, 1460 mol/m^3; □ $S_0(3)$, 148.5 K, 1890 mol/m^3; ○ $S_0(1)$, 41.5 K, 4950 mol/m^3; + $S_0(2)$, 148.5 K, 3550 mol/m^3.

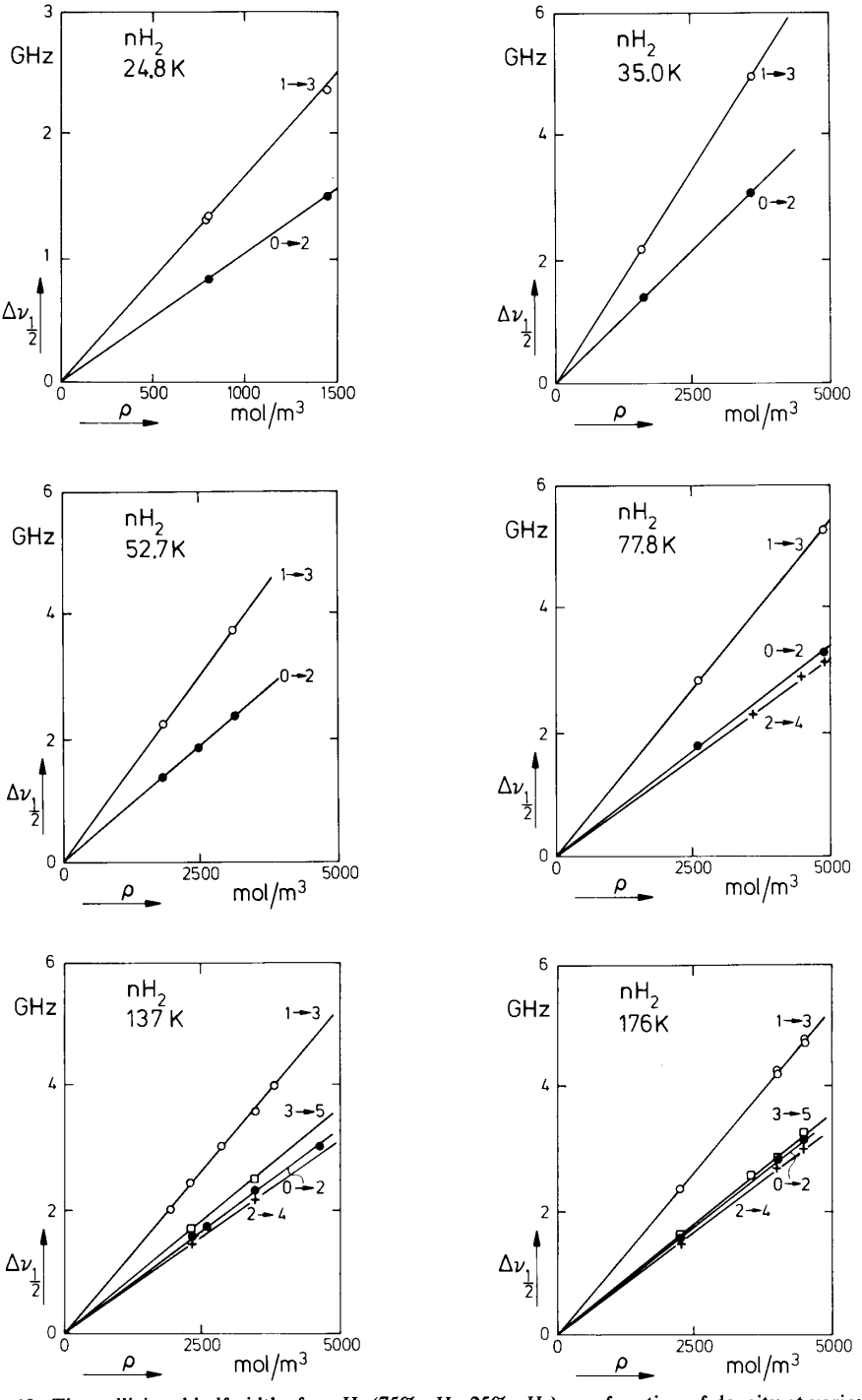

Fig. 10. The collisional halfwidths for nH_2 (75% oH_2–25% pH_2) as a function of density at various temperatures. 1 mol/m^3 corresponds to 0.02241 amagat; 1 amagat corresponds to 44.615 mol/m^3. ● $S_0(0)$; ○ $S_0(1)$; +$S_0(2)$; □ $S_0(3)$.

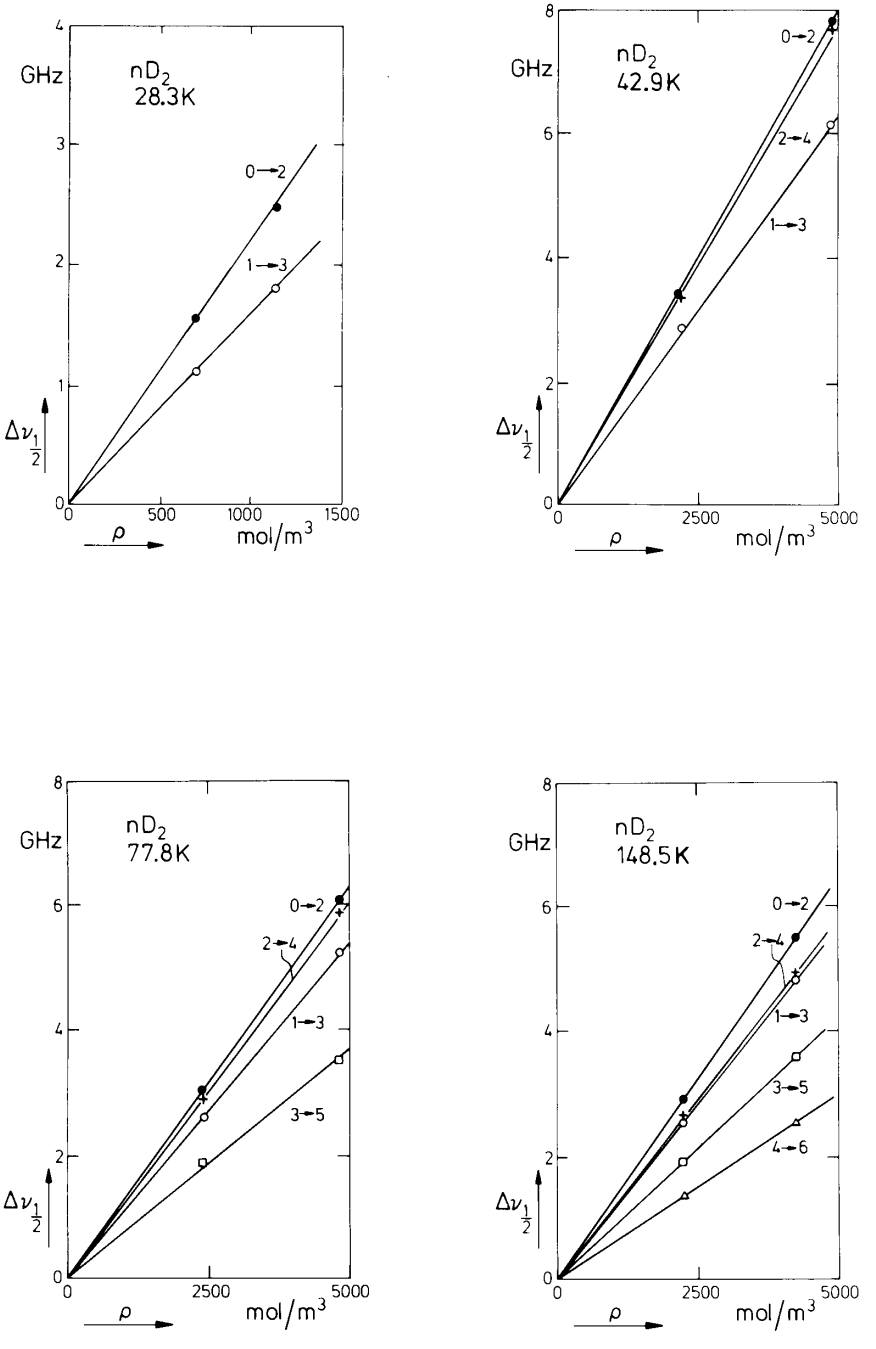

Fig. 11. The collisional halfwidths for nD_2 (67% oD_2–33% pD_2) as a function of density at various temperatures. ● $S_0(0)$; ○ $S_0(1)$; + $S_0(2)$; □ $S_0(3)$; △ $S_0(4)$.

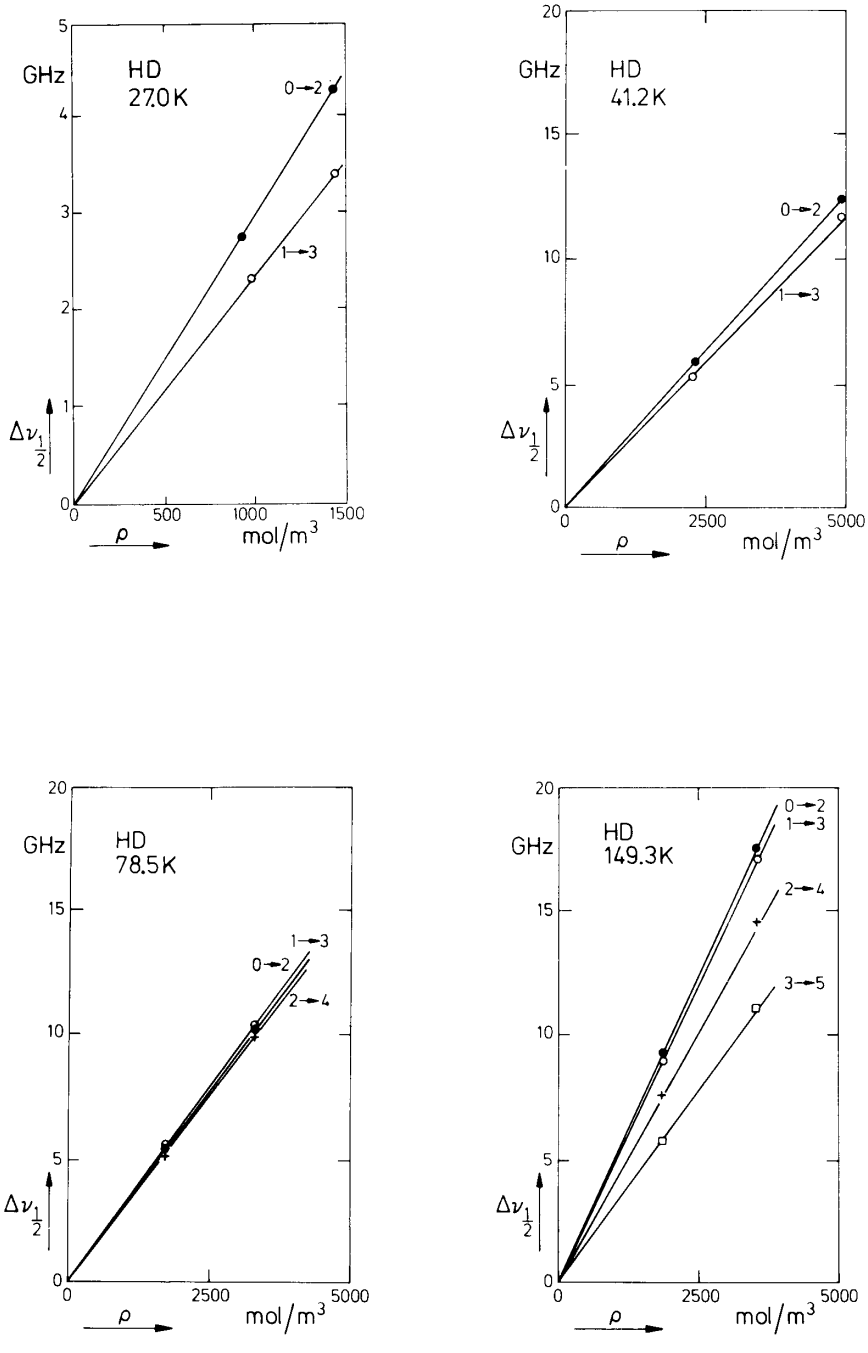

Fig. 12. The collisional halfwidths for HD as a function of density at various temperatures. ● $S_0(0)$; ○ $S_0(1)$; + $S_0(2)$; □ $S_0(3)$.

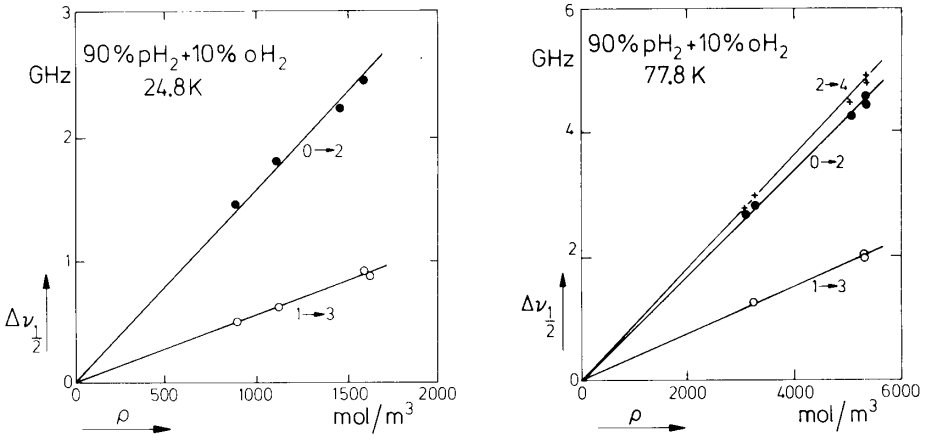

Fig. 13. The collisional halfwidths for the mixture 90% pH_2–10% oH_2 as a function of density at 24.8 K and 77.8 K. ● $S_0(0)$; ○ $S_0(1)$; + $S_0(2)$.

In figs. 10–14 the collisional halfwidths $\Delta\nu_{1/2}$ are presented as a function of the gas density. The collisional halfwidths of the rotational Raman lines were found to be proportional to the density within the experimental error.

From the slopes of the lines in figs. 10–14 the broadening coefficients $\Delta\nu_{1/2}/\rho$ were determined. For nH_2, nD_2 and HD these data are given in table I, where

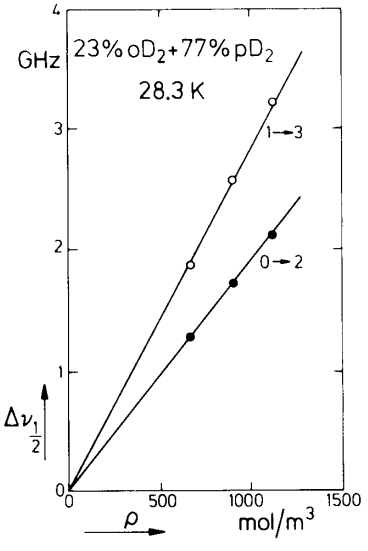

Fig. 14. The collisional halfwidths for the mixture 23% oD_2–77% pD_2 as a function of density at 28.3 K. ● $S_0(0)$; ○ $S_0(1)$.

TABLE I
Line broadening coefficients $\Delta\nu_{1/2}/\rho$ in MHz m^3/mol[a]

T(K)	$S_0(0)$	$S_0(1)$	$S_0(2)$	$S_0(3)$	$S_0(4)$	$S_0(5)$
			nH_2 (25.1% pH_2)			
293[b]	0.94 ± 0.02	1.17 ± 0.02	0.83 ± 0.02	0.85 ± 0.02	0.52 ± 0.02	
176	0.71 ± 0.01	1.06 ± 0.01	0.68 ± 0.01	0.73 ± 0.02	–	
137	0.66 ± 0.02	1.04 ± 0.02	0.63 ± 0.02	0.73 ± 0.02	–	
77.8	0.70 ± 0.01	1.11 ± 0.01	0.65 ± 0.02	–	–	
52.7	0.75 ± 0.01	1.20 ± 0.02	–	–	–	
35.0	0.87 ± 0.01	1.39 ± 0.01	–	–	–	
24.8	1.04 ± 0.01	1.65 ± 0.02	–	–	–	
			nD_2 (66.7% oD_2)			
293[b]	1.88 ± 0.02	1.50 ± 0.02	1.39 ± 0.02	1.14 ± 0.02	0.96 ± 0.02	0.63 ± 0.02
148.5	1.28 ± 0.01	1.12 ± 0.01	1.15 ± 0.01	0.84 ± 0.01	0.60 ± 0.02	–
77.8	1.25 ± 0.01	1.08 ± 0.01	1.21 ± 0.01	0.74 ± 0.02	–	–
42.9	1.59 ± 0.02	1.27 ± 0.03	1.57 ± 0.1	–	–	–
28.3	2.16 ± 0.03	1.58 ± 0.02	–	–	–	–
			HD			
293[b]	9.6 ± 0.2	8.5 ± 0.2	7.4 ± 0.2	6.1 ± 0.2	4.5 ± 0.2	
149.3	4.93 ± 0.1	4.80 ± 0.1	4.06 ± 0.05	3.1 ± 0.1	–	
78.5	3.03 ± 0.05	3.09 ± 0.05	2.94 ± 0.05	–	–	
41.2	2.53 ± 0.05	2.35 ± 0.05	–	–	–	
27.0	2.91 ± 0.05	2.33 ± 0.05	–	–	–	

[a] 1 MHz m^3/mol corresponds to 44.62 MHz/amagat.
[b] The data at 293 K are taken from ref. 7.

the broadening coefficients at room temperature, as measured by Keijser et al.[7]), are also included.

In figs. 15 and 16 the broadening coefficients are plotted as a function of the ortho–para composition for both H_2 and D_2. In the binary collision regime, these are linear functions of the concentration (see also the experiments of Keijser et al.[7])). The line broadening coefficients, obtained by extrapolation to the limit of the pure ortho and para modifications, are presented in table II.

For a discussion of the observed behavior of the line broadening in terms of molecular collision processes, it is useful to express the collisional broadening coefficients in terms of effective cross sections according to the relation

$$\mathfrak{S}_{RR} = \frac{2\pi\Delta\nu_{1/2}}{n\langle v\rangle}. \tag{10}$$

In this formula, n is the number density and $\langle v\rangle$ is the average relative velocity given by

$$\langle v\rangle = \sqrt{8k_B T/\pi\mu}. \tag{11}$$

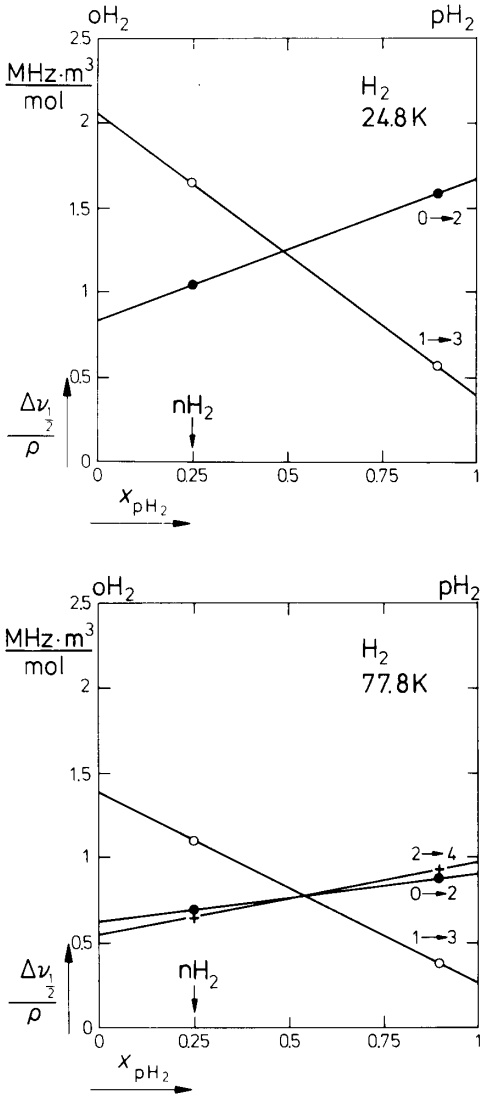

Fig. 15. The line broadening coefficients for H_2 as a function of the ortho–para composition at 24.8 K and 77.8 K. ● $S_0(0)$; ○ $S_0(1)$.

k_B is Boltzmann's constant, T is the absolute temperature and μ the reduced mass of the collision partners.

The Raman line broadening cross sections are presented in tables III and IV. In figs. 17–21 the cross sections are plotted as a function of the temperature. Some general trends are evident in these pictures. Especially at higher temperature, the cross sections for HD are considerably larger than

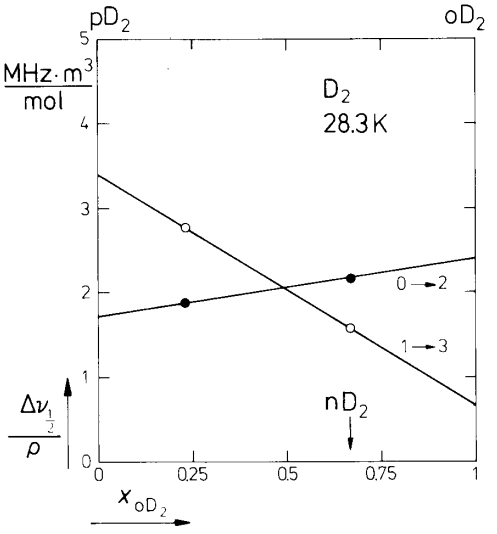

Fig. 16. The line broadening coefficients for D_2 as a function of the ortho–para composition at 28.3 K. ● $S_0(0)$; ○ $S_0(1)$.

TABLE II

Line broadening coefficients $\Delta\nu_{1/2}/\rho$ in MHz m^3/mol[a]

T(K)	$S_0(0)$	$S_0(1)$	$S_0(2)$	$S_0(3)$	$S_0(4)$
			oH_2		
293[b]	0.85 ± 0.02	1.28 ± 0.02	0.76 ± 0.02	0.92 ± 0.02	0.52 ± 0.02
77.8	0.63 ± 0.02	1.39 ± 0.02	0.55 ± 0.03	–	–
24.8	0.84 ± 0.02	2.06 ± 0.03	–	–	–
			pH_2		
293[b]	1.17 ± 0.02	0.74 ± 0.02	1.03 ± 0.02	0.61 ± 0.02	0.54 ± 0.02
77.8	0.91 ± 0.03	0.26 ± 0.02	0.99 ± 0.05	–	–
24.8	1.68 ± 0.07	0.40 ± 0.02	–	–	–
			pD_2		
28.3	1.73 ± 0.02	3.41 ± 0.05			
			oD_2		
28.3	2.38 ± 0.05	0.67 ± 0.05			

[a] 1 MHz m^3/mol corresponds to 44.62 MHz/amagat.

[b] The data at 293 K are taken from ref. 7.

TABLE III

Line broadening cross sections $\mathcal{G}_{RR}$ in 10^{-20} m^2

T(K)	$S_0(0)$	$S_0(1)$	$S_0(2)$	$S_0(3)$	$S_0(4)$	$S_0(5)$
			nH_2 (25.1% pH_2)			
293[a]	0.40 ± 0.01	0.49 ± 0.01	0.35 ± 0.01	0.36 ± 0.01	0.22 ± 0.01	
176	0.384 ± 0.005	0.576 ± 0.005	0.369 ± 0.005	0.39[4] ± 0.01	–	
137	0.40[8] ± 0.01	0.64[2] ± 0.01	0.38[4] ± 0.01	0.44[6] ± 0.01	–	
77.8	0.57 ± 0.01	0.90 ± 0.01	0.54 ± 0.02	–	–	
52.7	0.74 ± 0.02	1.19 ± 0.02	–	–	–	
35.0	1.06 ± 0.02	1.70 ± 0.02	–	–	–	
24.8	1.51 ± 0.02	2.38 ± 0.04	–	–	–	
			nD_2 (66.7%oD_2)			
293[a]	1.12 ± 0.01	0.89 ± 0.01	0.83 ± 0.01	0.68 ± 0.01	0.57 ± 0.01	0.37 ± 0.01
148.5	1.07 ± 0.01	0.94 ± 0.01	0.96 ± 0.01	0.70 ± 0.01	0.50 ± 0.02	–
77.8	1.45 ± 0.02	1.24 ± 0.02	1.40 ± 0.02	0.85 ± 0.05	–	–
42.9	2.47 ± 0.05	1.98 ± 0.05	2.44 ± 0.1[5]	–	–	–
28.3	4.13 ± 0.1	3.03 ± 0.05	–	–	–	–
			HD			
293[a]	4.9 ± 0.1	4.4 ± 0.1	3.8 ± 0.1	3.1 ± 0.1	2.3 ± 0.1	
149.3	3.56 ± 0.05	3.46 ± 0.05	2.93 ± 0.05	2.2[5] ± 0.1	–	
78.5	3.01 ± 0.05	3.08 ± 0.05	2.92 ± 0.05	–	–	
41.2	3.48 ± 0.1	3.23 ± 0.1	–	–	–	
27.0	4.94 ± 0.1	3.96 ± 0.1	–	–	–	

[a] The data at 293 K are taken from ref. 7.

TABLE IV

Line broadening cross sections $\mathcal{G}_{RR}$ in 10^{-20} m^2

T(K)	$S_0(0)$	$S_0(1)$	$S_0(2)$	$S_0(3)$	$S_0(4)$
			oH_2		
293[a]	0.36 ± 0.01	0.54 ± 0.01	0.32 ± 0.01	0.39 ± 0.01	0.22 ± 0.01
77.8	0.51 ± 0.02	1.13 ± 0.02	0.45 ± 0.03	–	–
24.8	1.21 ± 0.05	2.98 ± 0.05	–	–	–
			pH_2		
293[a]	0.49 ± 0.01	0.31 ± 0.01	0.43 ± 0.01	0.25 ± 0.01	0.23 ± 0.01
77.8	0.74 ± 0.03	0.22 ± 0.02	0.80 ± 0.05	–	–
24.8	2.41 ± 0.1	0.58 ± 0.02	–	–	–
			pD_2		
28.3	3.30 ± 0.05	6.5 ± 0.1			
			oD_2		
28.3	4.55 ± 0.1	1.29 ± 0.1			

[a] The data at 293 K are taken from ref. 7.

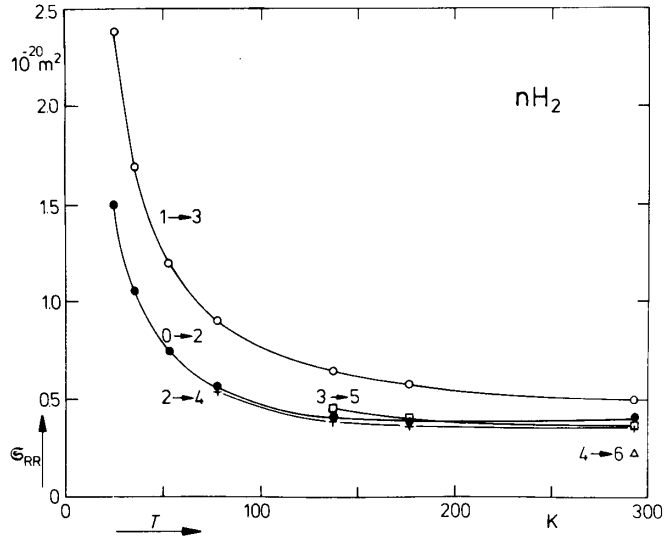

Fig. 17. The line broadening cross sections for nH_2 as a function of temperature. ● $S_0(0)$; ○ $S_0(1)$; + $S_0(2)$; □ $S_0(3)$; △ $S_0(4)$.

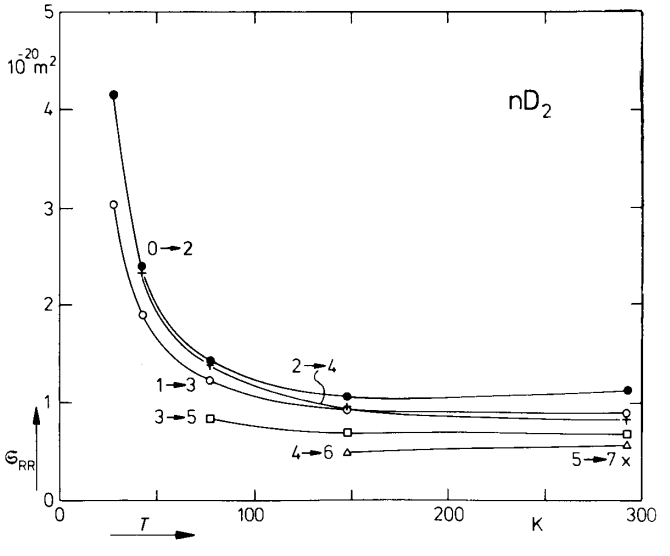

Fig. 18. The line broadening cross sections for nD_2 as a function of temperature. ● $S_0(0)$; ○ $S_0(1)$; + $S_0(2)$; □ $S_0(3)$; △ $S_0(4)$; × $S_0(5)$.

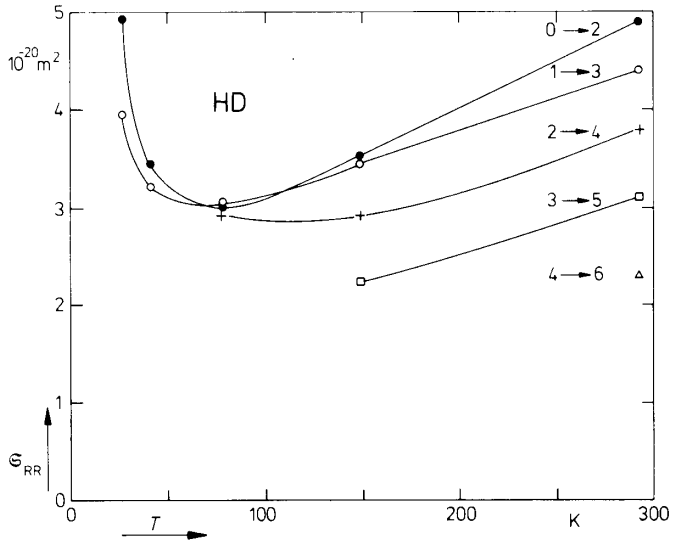

Fig. 19. The line broadening cross sections for HD as a function of temperature. ● $S_0(0)$; ○ $S_0(1)$; + $S_0(2)$; □ $S_0(3)$; △ $S_0(4)$.

those for the two homonuclear isotopes H_2 and D_2. The cross sections measured for D_2 are about a factor two larger than the corresponding H_2 cross sections. Towards lower temperature the cross sections increase sharply. For HD, a decrease as a function of J_i is observed, a tendency that is commonly found for other gases[20]). The dependence of the cross sections of H_2 and D_2 on J_i is rather complicated.

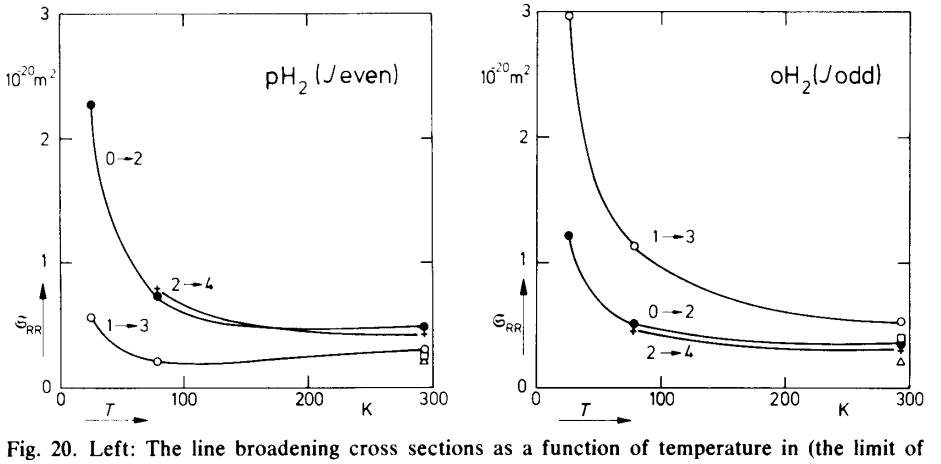

Fig. 20. Left: The line broadening cross sections as a function of temperature in (the limit of pure) pH_2. ● $S_0(0)$; 0 $S_0(1)$; + $S_0(2)$; □ $S_0(3)$; △ $S_0(4)$. Right: The line broadening cross sections as a function of temperature (in the limit of pure) oH_2. ● $S_0(0)$; 0 $S_0(1)$; + $S_0(2)$; □ $S_0(3)$; △ $S_0(4)$.

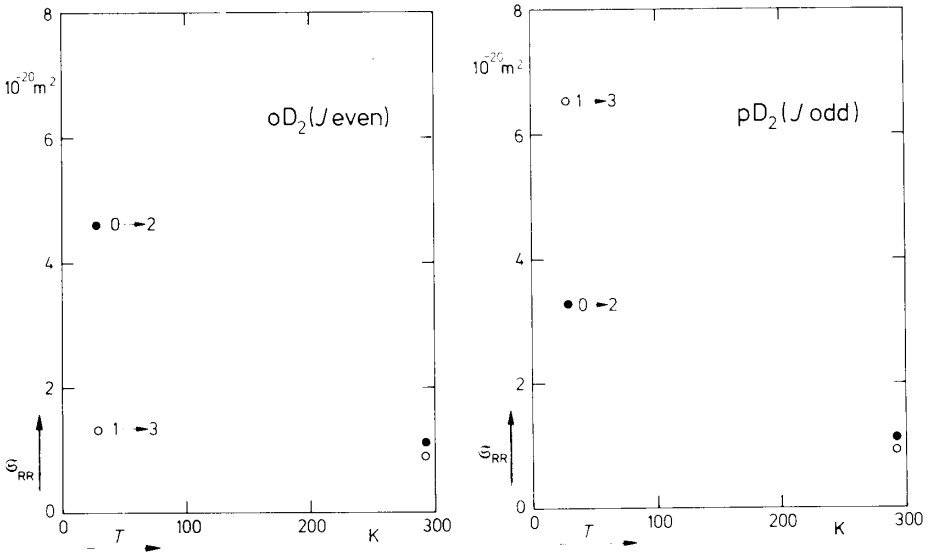

Fig. 21. The line broadening cross sections in (the limits of pure) oD_2 and pD_2. Experiments as a function of the ortho–para composition have only been performed at 28.3 K. For comparison cross sections in nD_2 at 293 K have been included. ● $S_0(0)$; ○ $S_0(1)$.

3.2. *Collisional line shift*

Following the procedure described in section 2.3 the line shift coefficients $\Delta\nu_S/\rho$ were calculated from the interferometer scanning gas pressure. $\Delta\nu_S$ is the difference between the central line frequency at density ρ and the frequency at zero density. The sign of $\Delta\nu_S$ is negative when the Raman line moves away from the exciting frequency with increasing density. In table V the collisional line shift coefficients are given for the rotational Raman lines of nH_2, nD_2 and HD. For the ortho–para mixtures of H_2 and D_2 with high para concentration, no reliable results on the line shift have been obtained. The only collisional line shift data on the rotational Raman lines of hydrogen available in the literature are the shift coefficients for the $S_0(0)$ and the $S_0(1)$ line in nH_2 at room temperature, as measured by Cooper et al.[21]). These values have been included in table V and fit well in the trend displayed by the data presented here.

The collisional line shift coefficients can be expressed as effective cross sections, analogously to eq. (10)

$$\mathfrak{S}^{S}_{RR} = \frac{2\pi\Delta\nu_S}{n\langle v\rangle}. \tag{12}$$

The line shift cross sections are given in table VI and are plotted as a function

TABLE V
Line shift coefficients $\Delta\nu_s/\rho$ in MHz m^3/mol[a]

T(K)	$S_0(0)$	$S_0(1)$	$S_0(2)$	$S_0(3)$	$S_0(4)$
		nH_2			
293[b]	-0.07 ± 0.03	-0.09 ± 0.03	–	–	
176	0.2	0.2	0.2	(0.6)	
137	0.4	0.3	–	(0.8)	
77.8	0.5	0.4	0.4	–	
52.7	0.6	0.7	–	–	
35.0	1.0	1.0	–	–	
27.7	1.0	1.1	–	–	
24.8	1.3	1.1	–	–	
20.2	1.5	1.4	–	–	
		nD_2			
148.5	0.0	−0.3	−0.2	0.1	(0.6)
77.8	0.4	−0.3	−0.2	0.6	–
42.9	0.7	−0.1	–	–	–
28.3	1.4	0.5	–	–	
		HD			
149.3	−1.8	−2.2	−1.2	(−0.1)	
78.5	−1.1	−1.5	−0.8	–	
41.2	−0.3	−1.1	–	–	
27.0	(−0.5)	(−0.8)	–	–	

[a] 1 MHz m3/mol corresponds to 44.62 MHz/amagat.
[b] The data at 293 K are taken from ref. 21.

The accuracy of the data is discussed in the text.

of the temperature in figs. 22–24. Positive as well as negative values are found for these cross sections. Practically all cross sections tend towards higher values at low temperature. A comparison with the corresponding line broadening cross sections show that $\mathfrak{S}^S_{RR}$ is in general somewhat smaller than $\mathfrak{S}_{RR}$.

At present no theoretical calculations are available for the collisional line shift cross sections for hydrogen–hydrogen systems. In ref. 22, Shafer and Gordon gave an extensive discussion about their results from close-coupling calculations on the collisional line shift for the $S_0(0)$ and $S_0(1)$ lines in H_2–He mixtures. Contributions to the cross section from the spherical and the nonspherical part of the intermolecular potential were found to be comparable in magnitude. The obtained cross sections were, however, extremely sensitive to the precise shape of the potential used. It will therefore not be attempted to give a qualitative interpretation of the measured line shift cross sections in terms of molecular interactions.

TABLE VI
Line shift cross sections $\mathcal{S}^{s}_{RR}$ in 10^{-20} m^2

T(K)	$S_0(0)$	$S_0(1)$	$S_0(2)$	$S_0(3)$	$S_0(4)$
293[a])	−0.028	−0.042	–	–	
176	0.1	0.1	0.1	(0.3)	
137	0.3	0.2	–	–	
77.8	0.4	0.4	0.4	(0.5)	
52.7	0.6	0.7	–	–	
35.0	1.3	1.2	–	–	
27.7	1.4	1.5	–	–	
24.8	1.9	1.7	–	–	
20.2	2.4	2.2	–	–	
		nD_2			
148.5	−0.0	−0.3	−0.2	0.1	(0.5)
77.8	0.4	−0.3	−0.2	0.7	–
42.9	1.1	−0.1	–	–	–
28.3	2.7	0.9	–	–	–
		HD			
149.3	−1.3	−1.6	−0.8	(−0.1)	
78.5	−1.1	−1.4	−0.8	–	
41.2	−0.4	−1.5	–	–	
27.0	(1.0)	(−1.4)	–	–	

[a] The data at 293 K are taken from ref. 21.

The accuracy of the data is discussed in the text.

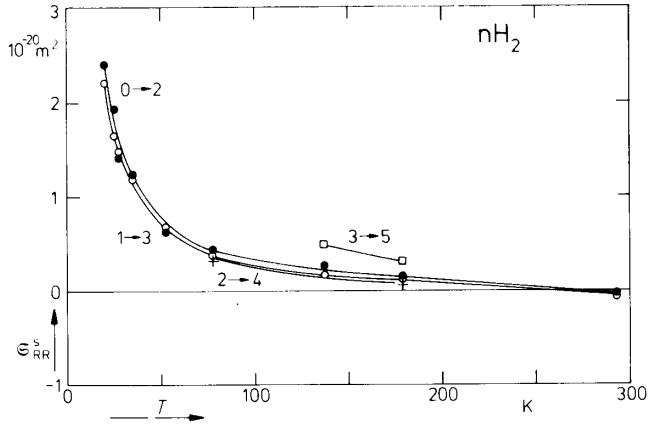

Fig. 22. The line shift cross sections for nH_2 as a function of temperature. ● $S_0(0)$; ○ $S_0(1)$; + $S_0(2)$; □ $S_0(3)$.

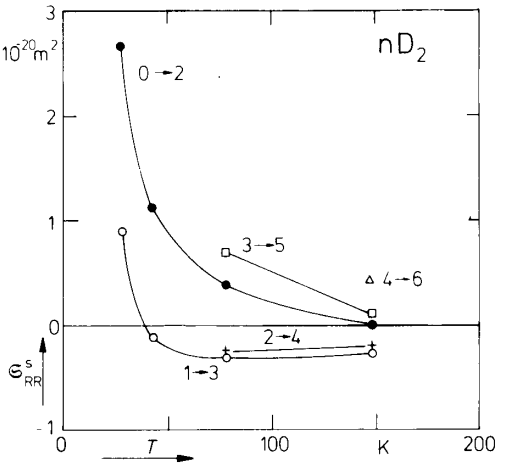

Fig. 23. The line shift cross sections for nD_2 as a function of temperature. ● $S_0(0)$; ○ $S_0(1)$; + $S_0(2)$; □ $S_0(3)$; △ $S_0(4)$.

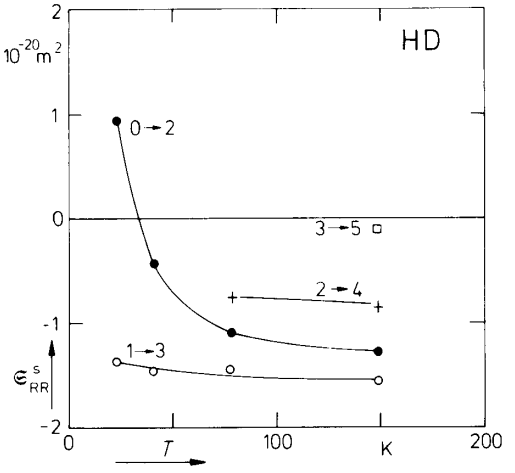

Fig. 24. The line shift cross sections for HD as a function of temperature. ● $S_0(0)$; ○ $S_0(1)$; + $S_0(2)$; □ $S_0(3)$.

4. Discussion

In refs. 22–24 general expressions are given which relate the line broadening cross sections to the intermolecular potential. Such expressions do not lend themselves very conveniently to the direct calculation of the line broadening cross sections. Neither are they convenient to serve as a basis for

a discussion of the experimentally observed behavior in terms of collision processes. We shall therefore introduce some well-known simplifying assumptions.

The intermolecular interaction is expanded in terms of the spherical harmonics of the orientations of the internuclear axes r_1 and r_2 of the two molecules (where the index 1 refers to the radiating molecule) and of the intermolecular axis $\boldsymbol{R}$, a vector between the molecular centers of charge (see fig. 25)[25-27]):

$$V(\boldsymbol{r}_1, \boldsymbol{r}_2, \boldsymbol{R}) = \sum_{L_1 L_2 L} V_{L_1 L_2 L}(\boldsymbol{r}_1, \boldsymbol{r}_2, \boldsymbol{R}), \tag{13}$$

where, for rigid rotors,

$$V_{L_1 L_2 L}(\boldsymbol{r}_1, \boldsymbol{r}_2, \boldsymbol{R}) = A_{L_1 L_2 L}(R) \sum_{M_1 M_2 M} \langle L_1 M_1 L_2 M_2 | L M \rangle \times Y_{L_1}^{M_1}(\hat{\boldsymbol{r}}_1) Y_{L_2}^{M_2}(\hat{\boldsymbol{r}}_2) Y_L^{M*}(\hat{\boldsymbol{R}}). \tag{14}$$

$\langle L_1 M_1 L_2 M_2 | L M \rangle$ is a Clebsch–Gordan coefficient and $\hat{\boldsymbol{r}}$ denotes a unit vector in the direction of $\boldsymbol{r}$. The strength $A_{L_1 L_2 L}(R)$ is dependent only on the intermolecular distance R. For the orders of the spherical harmonics, one has the general restriction[27])

$$L_1 + L_2 + L = \text{even},$$

and, furthermore,

L_1 and L_2 are even for homonuclear molecules.

Usually, not more than three terms are considered to be important for H_2 and D_2:

$$V^{\text{homonuclear}}(\boldsymbol{r}_1, \boldsymbol{r}_2, \boldsymbol{R}) = V_{000}(R) + V_{202}(\boldsymbol{r}_1, \boldsymbol{r}_2, \boldsymbol{R}) + V_{224}(\boldsymbol{r}_1, \boldsymbol{r}_2, \boldsymbol{R}). \tag{15}$$

$V_{000}(R)$ is the spherical potential; the other terms represent the anisotropic part of the potential. The electrostatic quadrupole–quadrupole interaction is of the form V_{224}. The term V_{022} has been omitted since, being spherical in the coordinates of the radiating molecule, it does not contribute to the line

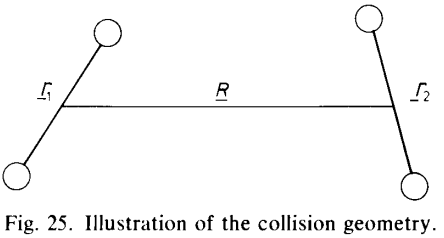

Fig. 25. Illustration of the collision geometry.

broadening[28]). Because the electronic configurations are virtually identical for H_2 and D_2, the potentials for the two isotopes can, to a good approximation, be considered to be the same.

For HD, where the nuclei are not identical, the molecular center of mass does not coincide with the center of electronic charge and consequently an extra angle dependent term in the potential is present[28–30]):

$$V^{\mathrm{HD}}(r_1, r_2, \boldsymbol{R}) = V^{\mathrm{homonuclear}}(r_1, r_2, \boldsymbol{R}) + V_{101}(r_1, r_2, \boldsymbol{R}). \tag{16}$$

The $V_{101}(r_1, r_2, \boldsymbol{R})$ term is rather strong compared to the other anisotropic terms.

With the above assumption about the shape of the intermolecular potential, a perturbation treatment can be applied to the expressions for the line broadening cross sections. Much simpler equations are then obtained, in which the contributions of the various anisotropic potential terms become additive. Particularly for hydrogen isotopes, where the angle dependent terms in the potential are small compared to the spherical potential, such a treatment should be expected to be applicable. The rotational Raman line broadening cross sections for H_2 and D_2 can then be written as:

$$\mathfrak{S}_{\mathrm{RR}}^{\mathrm{homonuclear}} = \mathfrak{S}_{\mathrm{RR}}^{202} + \mathfrak{S}_{\mathrm{RR}}^{224}, \tag{17}$$

and, for HD, one obtains:

$$\mathfrak{S}_{\mathrm{RR}}^{\mathrm{HD}} = \mathfrak{S}_{\mathrm{RR}}^{\mathrm{homonuclear}} + \mathfrak{S}_{\mathrm{RR}}^{101}. \tag{18}$$

The only potential terms that enter in a term $\mathfrak{S}_{\mathrm{RR}}^{L_1L_2L}$ are $V_{000}(R)$ and $V_{L_1L_2L}(r_1, r_2, \boldsymbol{R})$.

An additional advantage is that, at this stage, selection rules for the collisional transitions can be derived. The collisional transitions that are allowed, are found to be:

$$\begin{aligned}
&\mathfrak{S}_{\mathrm{RR}}^{101}: \quad \Delta J_1 = \pm 1 \quad , \quad \Delta J_2 = 0;\\
&\mathfrak{S}_{\mathrm{RR}}^{202}: \quad \Delta J_1 = 0, \pm 2, \quad \Delta J_2 = 0;\\
&\mathfrak{S}_{\mathrm{RR}}^{224}: \quad \Delta J_1 = 0, \pm 2, \quad \Delta J_2 = 0, \pm 2,
\end{aligned}$$

where J_1 refers to the spectroscopic states of the radiator (J_i and J_f) and J_2 to the rotational state of the perturbing molecule. In the case of $\mathfrak{S}_{\mathrm{RR}}^{224}$, all combinations of the indicated transitions ΔJ_1 and ΔJ_2 are allowed; for the particular case $J_2 = 0$ and $\Delta J_2 = 0$, $\mathfrak{S}_{\mathrm{RR}}^{224}$ vanishes.

We shall now proceed with a discussion of the experimental cross sections as reported in section 3.1. It is seen in figs. 17–21, where the line broadening cross sections for the various hydrogen gases are depicted as a function of temperature, that the temperature dependence for HD is rather different from that for H_2 and D_2. It will be shown later that this is due to the important V_{101}

term in the HD potential. It is convenient to discuss first the homonuclear isotopes, where the cross sections are described by $\mathcal{S}_{RR}^{202}$ and $\mathcal{S}_{RR}^{224}$, and then consider the more complicated case of HD.

4.1. H_2 *and* D_2

For the present discussion it will prove to be useful to separate the collision processes that are relevant for the line broadening into elastic and inelastic collisions. A collision will be called *elastic* if no net exchange between rotational and translational energy takes place within the collision system. Two distinct types of elastic collisions are to be defined. *Resonance collisions* are collisions in which both molecules undergo a change in rotational energy, but in such a way that the sum of their rotational energies is preserved. *Elastic nonresonant collisions* are collision processes in which the J-quantum numbers describing the rotational states of each molecule, remain unchanged. A collision is called *inelastic*, if a net transfer of energy takes place between the rotational and translational degrees of freedom.

Shortly, it will be shown that the effect of inelastic collisions on the line broadening is small for H_2 and D_2, particularly at low temperatures. Consequently, only a small number of collisional transitions are relevant. It is instructive to summarize the elastic collisional transitions that can be important at low temperatures. In table VII it is indicated which cross sections $\mathcal{S}_{RR}^{L_1L_2L}$ of eq. (17) contribute to the broadening of the $S_0(0)$ and $S_0(1)$ lines.

A resonance collision cannot occur via a collision between an ortho and a para molecule because of the mismatch of the rotational energy spacings of the collision partners. Only via collisions between partners belonging to the same modification can such resonant transitions take place. In fig. 20 we see indeed that in pH_2 (a bath of even perturbers) the experimental cross sections

TABLE VII
Collisional contributions to line broadening for H_2 and D_2 at low temperature

	Spectroscopic transition ($J_i \to J_f$)	Resonant collisions	Elastic nonresonant collisions
$S_0(0)$ in pH_2 and oD_2 ($J_2 = 0$)	$(0 \to 2)$	$\mathcal{S}_{RR}^{224}$ J_f: $2 \to 0$, J_2: $0 \to 2$	$\mathcal{S}_{RR}^{202}$
$S_0(0)$ in oH_2 and pD_2 ($J_2 = 1$)	$(0 \to 2)$	–	$\mathcal{S}_{RR}^{202}$, $\mathcal{S}_{RR}^{224}$
$S_0(1)$ in pH_2 and oD_2 ($J_2 = 0$)	$(1 \to 3)$	–	$\mathcal{S}_{RR}^{202}$
$S_0(1)$ in oH_2 and pD_2 ($J_2 = 1$)	$(1 \to 3)$	$\mathcal{S}_{RR}^{224}$ J_f: $3 \to 1$, J_2: $1 \to 3$	$\mathcal{S}_{RR}^{202}$, $\mathcal{S}_{RR}^{224}$

for the $S_0(0)$ and $S_0(2)$ lines, involving even rotational states, are appreciably larger than those for the $S_0(1)$ line (connecting odd levels). For oH_2, on the other hand, the $S_0(1)$ line is broader than the $S_0(0)$ and the $S_0(2)$ lines.

For the elastic nonresonant collisions it is seen in table VII that the contribution of $\mathcal{G}_{RR}^{224}$ vanishes in the case of pH_2. We can now understand why the $S_0(1)$ cross section is much more sensitive to the ortho–para composition than the cross section for the $S_0(0)$ line: for the $S_0(1)$ line both the resonant and elastic nonresonant contributions increase with increasing oH_2 concentration. For the $S_0(0)$ line, the two contributions have an opposite concentration dependence.

For the cross sections for D_2 at 28.3 K (fig. 21) a similar dependence on the rotational states is observed.

Next we consider the dependence on the temperature and the molecular mass. In the low temperature region, all cross sections increase markedly towards lower temperature. The cross sections for D_2 are larger than the corresponding H_2 cross sections. In fig. 26 $\mathcal{G}_{RR}Tm^{-1}$ is plotted as a function of the temperature below 80 K. By comparing the corresponding cross sections for the different modifications, it is seen that the behavior of the cross sections as a function of temperature and mass is fairly well described by $\mathcal{G}_{RR} \propto mT^{-1}$.

We can gain insight about this dependence by considering the matrix elements involved in the expression for the line broadening cross section, which can, for a classical trajectory, be expressed in time dependent pertur-

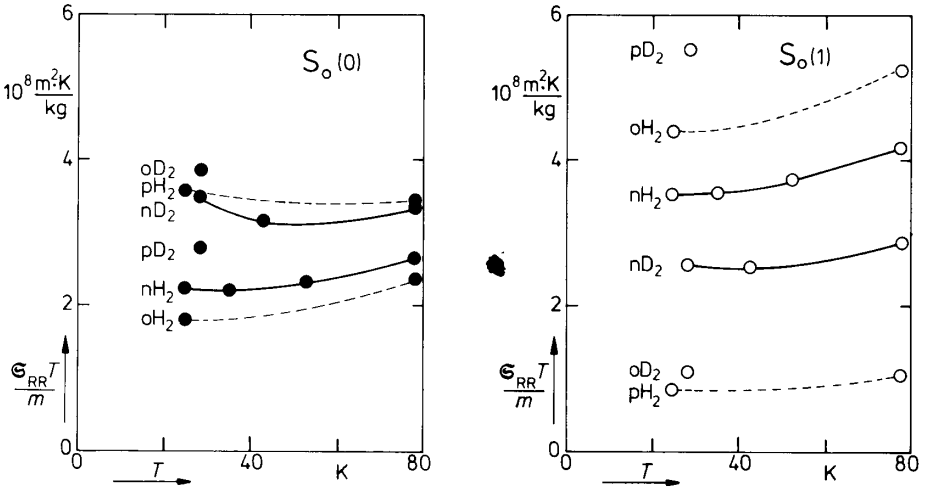

Fig. 26. $\mathcal{G}_{RR}Tm^{-1}$ as a function of temperature for the $S_0(0)$ and the $S_0(1)$ lines of H_2 and D_2.

bation theory in the form[23]):

$$\langle J_1' J_2' | T | J_1 J_2 \rangle \propto \int_{-\infty}^{\infty} e^{i\hbar^{-1}\Delta E t} \langle J_1' J_2' | V^{\text{anis}}(t) | J_1 J_2 \rangle \, dt. \tag{19}$$

Here, ΔE is the total rotational energy change occurring at the collision considered, and $V^{\text{anis}}(t)$ is the anisotropic part of the intermolecular potential. For elastic collisions ($\Delta E = 0$), the integrand depends on t only through $V^{\text{anis}}(t)$. In the case of straight line trajectories with constant velocity v, the argument t of V^{anis} enters only in the combination vt. The integral in eq. (19) is then proportional to v^{-1}. The line broadening cross section is a sum of terms containing a product of two matrix elements. Hence we find in this simple picture, after Boltzmann averaging over the velocities, that $\mathfrak{S}_{\text{RR}} \propto \langle v \rangle^{-2} \propto mT^{-1}$, provided that the distribution of the perturbers over the rotational states is constant.

For the hydrogen isotopes a more realistic approach is based upon the Distorted Wave Born Approximation (DWBA)[31]). In this approximation the spherical wave functions, describing the relative translational motion, are calculated in an exact quantum mechanical manner (or at least in a high order perturbation treatment when certain approximations are used) from the spherical part of the potential, $V_{000}(R)$. These wave functions are then used to calculate the transition matrix elements to first order in the nonspherical potential. The DWBA is often used under conditions for which the cross sections to be calculated are small compared to the total kinetic cross sections. Because of the small nonsphericity in the potential for hydrogen isotopes, the DWBA is often applied for these systems. Calculations with the DWBA have been performed by a.o. Moraal[32]) and Coombe and Köhler[33]).

An expression is obtained for the cross sections in eq. (13) which can be written schematically as[33,34])

$$\begin{aligned} \mathfrak{S}_{\text{RR}}^{L_1 L_2 L}(J_i, J_f; J_i, J_f) = \sum_{J_2 J_2'} p_{J_2} K_1(J_2 J_2' L_2) \times \Bigg[& \sum_{J_i' \neq J_i} K_2(J_i J_i' L_1) \hat{\mathfrak{S}}_{L_1 L_2 L}(\beta \Delta E_{J_i' J_2' J_i J_2}) \\ & + \sum_{J_f' \neq J_f} K_2(J_f J_f' L_1) \hat{\mathfrak{S}}_{L_1 L_2 L}(\beta \Delta E_{J_f' J_2' J_f J_2}) \\ & + K_3(J_i J_f L_1) \hat{\mathfrak{S}}_{L_1 L_2 L}(\beta \Delta E_{J_2' J_2}) \Bigg]. \end{aligned} \tag{20}$$

Here the following definitions have been used

$$\beta = (k_B T)^{-1}; \tag{21}$$

$$\Delta E_{J_1 J_2 J_3 J_4} = E_{J_1} + E_{J_2} - E_{J_3} - E_{J_4}; \tag{22}$$

$$\Delta E_{J_1J_2} = E_{J_1} - E_{J_2}; \tag{23}$$

$$E_J = BJ(J+1), \tag{24}$$

where B is the rotational constant. Each term in eq. (20) refers to a particular type of collision, where J_i and J_f are interpreted as the states involved in the spectroscopic transition of the radiator and J_2 as the rotational state of the perturber before the collision. The primes refer to post-collisional states. The factors $K_\alpha(J_1J_2L)$ are constants containing 3j-symbols and thus the collisional selection rules mentioned above.

An important advantage of the above expressions is that the shape of the potential term $V_{L_1L_2L}(R)$ enters, along with $V_{000}(R)$, only in the translational factors $\hat{\Im}_{L_1L_2L}(\beta\Delta E)$. This factor is dependent on the rotational J-states of the molecules only through the argument $\beta\Delta E$, which represents the total energy exchange (normalized by the thermal energy) between the rotational and the translational degrees of freedom.

In the DWBA calculation for H_2 as given by Moraal[32]), the spherical wave functions of an assumed hard sphere potential are further approximated, so that the radial integral over the V_{224} potential term can be evaluated analytically. Furthermore, only a crude estimate of the contribution of the V_{202} term in the intermolecular interaction is made. At 300 K good agreement is found for the $S_0(2)$, $S_0(3)$ and $S_0(4)$ lines, but for the $S_0(0)$ and $S_0(1)$ lines there were serious discrepancies (see fig. 27). No calculations were performed for lower temperatures or for D_2.

Recently, also Coombe and Köhler[33]) calculated the collisional line broadening on the basis of the DWBA, using a square well model for the

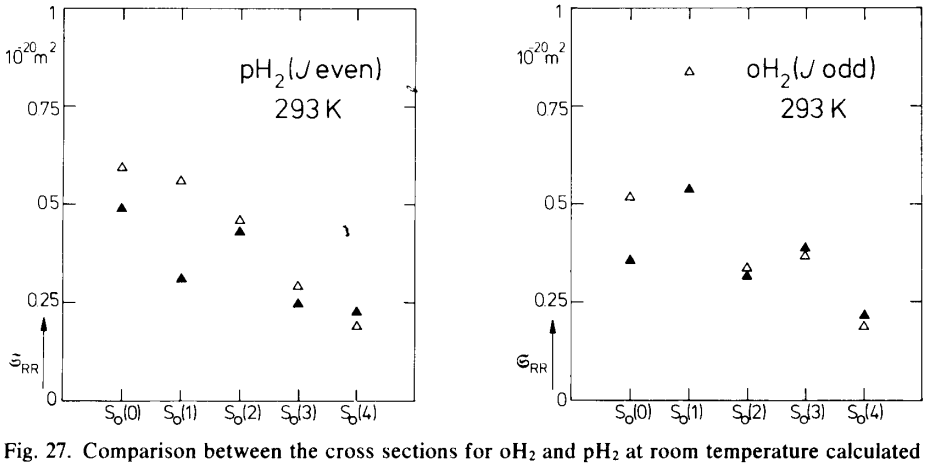

Fig. 27. Comparison between the cross sections for oH_2 and pH_2 at room temperature calculated by Moraal[32]) (△) and the experimental cross sections (▲).

spherical part of the interaction. Both $\mathfrak{S}_{RR}^{202}$ and $\mathfrak{S}_{RR}^{224}$ were evaluated without making further essential approximations. The square well parameters were adjusted to obtain the best fit with experimental data. In fig. 28 the calculated cross sections for oH_2 and pH_2 are shown together with the experimental results. It is seen that good agreement with the experiment is obtained in the whole temperature range from 20 K to 300 K. $\mathfrak{S}_{RR}^{202}$ was found to be very sensitive to the choice of the parameter that characterizes the repulsive wall diameter. Equally good agreement with the experiments for D_2 could be achieved only by slightly changing this parameter.

The low temperature results are particularly interesting since at low temperatures only very few elastic collisional processes play a role. From the low temperature measurements four linewidths have been derived: the widths of the $S_0(0)$ and the $S_0(1)$ lines both in purely ortho ($J = 1$ molecules) and in purely para ($J = 0$ molecules) hydrogen.

At low temperatures the expression of eq. (20) reduces to (see also the more explicit form of eq. (20) in ref. 32):

$$\mathfrak{S}_{RR}^{202} = \frac{3(4J_i^2 + 12J_i - 3)}{(2J_i - 1)(2J_i + 3)^2(2J_i + 7)} \hat{\mathfrak{S}}_{202}(0) + [\text{inelastic terms}] \tag{25}$$

and

$$\mathfrak{S}_{RR}^{224} = \left[3 \frac{J_2(J_2+1)}{(2J_2-1)(2J_2+3)} \frac{(4J_i^2 + 12J_i - 3)}{(2J_i-1)(2J_i+3)^2(2J_i+7)} - \frac{6}{49} \frac{(J_i+1)(J_i+2)}{(2J_i+3)^3(2J_i+1)} J_i^2 \delta_{J_iJ_2}\right] \hat{\mathfrak{S}}_{224}(0)$$

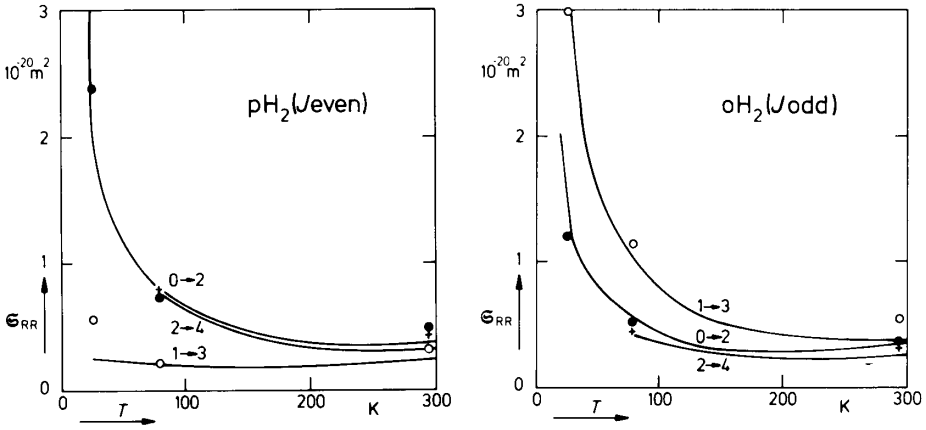

Fig. 28. Comparison between the cross sections as calculated by Coombe and Köhler[33]) and the experimental cross sections. Left: radiating molecule in a bath of pH_2. Right: Radiating molecule in a bath of oH_2. —— theory. ● $S_0(0)$; ○ $S_0(1)$; + $S_0(2)$.

$$+\frac{9}{8}\frac{(J_2+1)(J_2+2)}{(2J_2+1)(2J_2+3)}\frac{(J_i+1)(J_i+2)}{(2J_i+3)(2J_i+5)}$$
$$\times \exp[2\beta B(J_i-J_2)]\exp[-2\beta B|J_i-J_2|]\,\hat{\mathfrak{S}}_{224}(4\beta B|J_i-J_2|)$$
$$+[\text{inelastic terms}]. \qquad (26)$$

The expressions (25) and (26) are identical to the ones given by Moraal, except for the 2nd term of eq. (26), which Moraal gives as

$$+\frac{18}{49}\frac{(J_i+1)(J_i+2)}{(2J_i+3)}J_i\delta_{J_iJ_2},$$

but in practice the difference is of minor importance. J_f is written as J_i+2. The term containing $\hat{\mathfrak{S}}_{224}(4\beta B|J_i-J_2|)$ in eq. (26) refers to resonance collisions; when $J_i \neq J_2$, $\hat{\mathfrak{S}}_{224}(4\beta B|J_i-J_2|)$ is very small.

In particular, one gets for the four cross sections corresponding to the four linewidths at low temperature:

$$S_0(0)\text{ in pH}_2\text{: } \mathfrak{S}\left(\begin{matrix}0\to2\\ \text{para}\end{matrix}\right)=\frac{1}{7}\hat{\mathfrak{S}}_{202}(0)+\frac{1}{10}\hat{\mathfrak{S}}_{224}(0)+[\text{inelastic terms}]$$

$$S_0(1)\text{ in pH}_2\text{: } \mathfrak{S}\left(\begin{matrix}1\to3\\ \text{para}\end{matrix}\right)=\frac{13}{75}\hat{\mathfrak{S}}_{202}(0)+[\text{inelastic terms}]$$

$$S_0(0)\text{ in oH}_2\text{: } \mathfrak{S}\left(\begin{matrix}0\to2\\ \text{ortho}\end{matrix}\right)=\frac{1}{7}\hat{\mathfrak{S}}_{202}(0)+\frac{2}{35}\hat{\mathfrak{S}}_{224}(0)+[\text{inelastic terms}]$$

$$S_0(1)\text{ in oH}_2\text{: } \mathfrak{S}\left(\begin{matrix}1\to3\\ \text{ortho}\end{matrix}\right)=\frac{13}{75}\hat{\mathfrak{S}}_{202}(0)+\left(\frac{26}{375}-\frac{12}{6125}+\frac{27}{350}\right)\hat{\mathfrak{S}}_{224}(0)+[\text{inelastic terms}]. \qquad (27)$$

According to Moraal the coefficient of $\hat{\mathfrak{S}}_{224}(0)$ in the last line of eq. (27) is $(\frac{36}{375}+\frac{36}{1225}+\frac{27}{350})$.

As can be seen, these four cross sections are essentially determined by two parameters, $\hat{\mathfrak{S}}_{202}(0)$ and $\hat{\mathfrak{S}}_{224}(0)$. We have measured these four cross sections in H_2 at 24.8 K. This yields an overdetermined set of equations for $\hat{\mathfrak{S}}_{202}(0)$ and $\hat{\mathfrak{S}}_{224}(0)$.

We will first indicate how the corrections for the inelastic terms in eq. (27) are made. For three of the four mentioned cross sections, the inelastic contributions can be directly expressed – within the DWBA – in terms of $\mathfrak{S}(0001)$, the cross section obtained in rotational relaxation experiments[34]). This cross section has not been measured at low temperatures, but in ref. 35 a method is given to calculate $\mathfrak{S}(0001)$ from values measured at higher temperatures. The inelastic contributions are indeed found to be small (about 0.02×10^{-20} m^2). The one that cannot be calculated (for the $S_0(1)$ line in pH_2) is taken to be of the same magnitude.

After correcting for the small inelastic contribution, we can use eqs. (27) to calculate $\hat{\mathfrak{S}}_{202}(0)$ and $\hat{\mathfrak{S}}_{224}(0)$ from the experimental cross sections. $\hat{\mathfrak{S}}_{202}(0)$ can be directly obtained from the expression for $\mathfrak{S}(^{1\to3}_{\text{para}})$. We find $\hat{\mathfrak{S}}_{202}(0)=$

$(3.2 \pm 0.2) \times 10^{-20}$ m^2 (see table VIII). When this value is inserted in the three other equations of eq. (27), each gives a value of $\hat{\mathcal{C}}_{224}(0)$. In table VIII the values for $\hat{\mathcal{C}}_{202}(0)$ and $\hat{\mathcal{C}}_{224}(0)$ are given.

A similar calculation can be performed for H_2 at 77.8 K and for D_2 at 28.3 K. For H_2, the estimated corrections for the inelastic contributions are larger at 77.8 K than at 24.8 K: about 0.04×10^{-20} m^2. The inelastic contributions for D_2 at 28.3 K are taken to be a factor two larger than the corresponding H_2 values, in accordance with the (few) experimental data for $\mathcal{C}(0001)$ for D_2 [36]). The results for these systems are also included in table VIII. The indicated errors exclusively refer to the errors in the experimental line broadening cross sections and involve neither theoretical uncertainties nor errors associated with the estimation of the inelastic contributions.

It is seen in table VIII that the three values for $\hat{\mathcal{C}}_{224}(0)$ agree with each other at 77.8 K and also for D_2 at 28.3 K. For H_2 at 24.8 K the three values for $\hat{\mathcal{C}}_{224}(0)$ are of the same order of magnitude but they differ by about 30%. This is larger than the experimental error. One might be tempted to explain this discrepancy by arguing that the molecular wave functions have not been symmetrized in the derivation of eqs. (21) and (22). In ref. 19, however, in a similar analysis of the cross sections for the depolarized Rayleigh line, a distinct discrepancy is found between the value for $\hat{\mathcal{C}}_{202}(0)$ calculated here and the value obtained from the depolarized Rayleigh line broadening in (the limit of) pure pH_2. Since in both cases the cross sections refer to collisions of unlike particles (radiators in odd J states perturbed by molecules in state $J = 0$, the above explanation referring to symmetrization is clearly not appropriate. Another possibility is, that, apart from $\mathcal{C}_{RR}^{202}$ and $\mathcal{C}_{RR}^{224}$ in eq. (17), other terms in the cross section play a significant role. Thirdly, we mention as a possible explanation for the discrepancy that the DWBA might break down for the hydrogen molecules at low temperatures. Some evidence for this assumption is found in ref. 37, where the results obtained in DWBA cal-

TABLE VIII
Calculated values for $\hat{\mathcal{C}}_{202}(0)$ and $\hat{\mathcal{C}}_{224}(0)$ in 10^{-20} m^2

	$\hat{\mathcal{C}}_{202}(0)$*	$\hat{\mathcal{C}}_{224}(0)$**		
		a	b	c
H_2, 24.8 K	3.2 ± 0.2	19.2 ± 0.8	13.0 ± 0.8	16 ± 0.5
H_2, 77.8 K	0.9 ± 0.1	5.8 ± 0.3	5.9 ± 0.5	6.2 ± 0.2
D_2, 28.3 K	7.0 ± 0.7	35.2 ± 1.6	39.4 ± 1.6	34.9 ± 1.0

* Obtained from $\mathcal{C}_{RR}$ for $S_0(1)$ in pH_2 resp. oD_2.

** Obtained from $\hat{\mathcal{C}}_{202}(0)$ and a) $\mathcal{C}_{RR}$ for $S_0(0)$ in pH_2 resp. oD_2; b) $\mathcal{C}_{RR}$ for $S_0(0)$ in oH_2 resp. pD_2; c) $\mathcal{C}_{RR}$ for $S_0(1)$ in oH_2 resp. pD_2.

culations on the system H_2–He at 20 K were found to deviate considerably from the values obtained in exact calculations. A further discussion on these discrepancies will be given in ref. 19.

4.2. *HD*

The interpretation of the line broadening cross sections for HD is more complicated than for H_2 and D_2, where inelastic contributions could be neglected at low temperatures. In the case of HD one has to take into account not only the predominantly elastic processes connected with $\mathfrak{S}_{RR}^{\text{homonuclear}}$, but also the inelastic collisions associated with $\mathfrak{S}_{RR}^{101}$ (eq. (18)). The contribution of $\mathfrak{S}_{RR}^{101}$ to $\mathfrak{S}_{RR}$ is known to be the dominant one at room temperature[7,29]) but at lower temperatures it is certainly not possible to neglect $\mathfrak{S}_{RR}^{\text{homonuclear}}$, because the elastic line broadening cross sections strongly increase with decreasing temperature. A quantitative analysis, similar to the above treatment of H_2 and D_2, cannot be performed here, because for HD the number of cross sections known from experiments is smaller than the number of important translational factors.

In the following we will therefore adopt a somewhat different approach. Since the behavior of $\mathfrak{S}_{RR}^{\text{homonuclear}}$ is by now rather well understood from the discussion of the previous section on H_2 and D_2, a quantitative estimate can be made of $\mathfrak{S}_{RR}^{\text{homonuclear}}$ for HD. By subtracting this contribution from the experimental value for $\mathfrak{S}_{RR}$, one obtains $\mathfrak{S}_{RR}^{101}$ (eq. (18)).

In the low temperature range, $\mathfrak{S}_{RR}^{\text{homonuclear}}$ can be estimated from eqs. (25) and (26), because the values $\hat{\mathfrak{S}}_{202}(0)$ and $\hat{\mathfrak{S}}_{224}(0)$ are known to scale roughly proportional to the molecular mass. In the high temperature range, where about 50% of the HD molecules are in an even rotational state, a similar scaling of the cross section for a H_2 mixture containing 50% pH_2 can also be expected to give a rather good estimate for $\mathfrak{S}_{RR}^{\text{homonuclear}*}$. Although the described procedure cannot be expected to yield very accurate results for $\mathfrak{S}_{RR}^{\text{homonuclear}}$, even an appreciable error does not affect the values for $\mathfrak{S}_{RR}^{101}$ very much, since in most cases $\mathfrak{S}_{RR}^{101}$ is considerably larger than $\mathfrak{S}_{RR}^{\text{homonuclear}}$.

In fig. 29 the values for $\mathfrak{S}_{RR}^{101}$ calculated for 27 K, 78 K and 293 K are shown. The dotted lines connecting these points were drawn using the HD broadening cross sections measured at other temperatures, together with estimates for $\mathfrak{S}_{RR}^{\text{homonuclear}}$ obtained from interpolated values for oH_2 and pH_2.

* This procedure at high temperatures can be justified by examining the explicit form of eq. (18). As a check, the cross sections for nD_2 at room temperature were calculated in this way from the cross section for a corresponding H_2 mixture (33% oH_2–67% pH_2). The experimental values for nD_2 were thus reproduced with an accuracy of 10%.

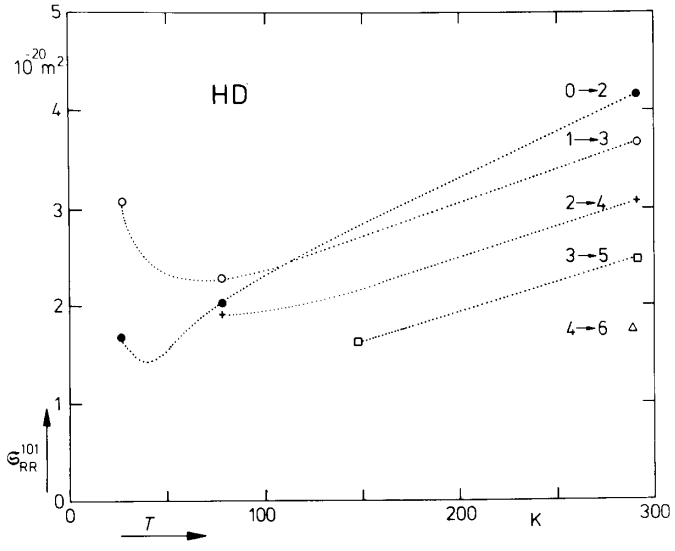

Fig. 29. Estimated $\mathcal{S}_{RR}^{101}$ as a function of temperature for HD.

At temperatures above 100 K the inelastic cross sections $\mathcal{S}_{RR}^{101}$ are seen to be increasing functions of the temperature. This is understandable, since at higher temperature the increased translational energy makes rotational–translational energy exchange more probable. Even at the lowest temperatures appreciable values for the cross sections are found. The magnitude is of the same order as $\mathcal{S}(0001)$ (2.6×10^{-20} m^2 [38]), which is essentially the inelastic cross section for deexcitation from $J = 1$ to $J = 0$.

At high temperatures the cross section decreases with increasing J_i. This is associated with the large energy level spacing at high values of the rotational quantum number, which makes inelastic transitions improbable for radiators in high rotational states.

Acknowledgements

The authors are indebted to Dr. D.A. Coombe of the University of British Columbia and Dr. W.E. Köhler of the University of Erlangen-Nürnberg for their continuous interest in this work and for making the results of their calculations available prior to publication. The continuous interest in this research of Prof. J.J.M. Beenakker and his many helpful discussions are gratefully acknowledged.

This work is part of the research program of the "Stichting voor Fun-

damenteel Onderzoek der Materie (FOM)" and has been made possible by financial support from the "Nederlandse Organisatie voor Zuiver-Wetenschappelijk Onderzoek (ZWO)".

References

1) B.J. Berne and R. Pecora, Dynamic Light Scattering (Wiley, New York, 1976).
2) H.F.P. Knaap and P. Lallemand, Ann. Rev. Phys. Chem. **26** (1975) 59.
3) C.G. Gray and H.L. Welsh, Essays in Structural Chemistry (Macmillan, London, 1971).
4) J. van Kranendonk, Can. J. Phys. **41** (1963) 433.
5) J.I. Gersten and H.F. Foley, J. Opt. Soc. Amer. **58** (1968) 933.
6) B.K. Gupta and A.D. May, Can. J. Phys. **50** (1972) 1747.
7) R.A.J. Keijser, J.R. Lombardi, K.D. van den Hout, B.C. Sanctuary and H.F.P. Knaap, Physica **76** (1974) 585.
8) R.A.J. Keijser, K.D. van den Hout, M. de Groot and H.F.P. Knaap, Physica **75** (1974) 515.
9) N.J. Bridge and A.D. Buckingham, Proc. Roy. Soc. (London) Ser. **A295** (1966) 334.
10) A. Fookson, P. Pomerantz and E.H. Rich, J. Res. Natl. Bur. Std. **47** (1951) 31.
11) D.A. Depatie and R.L. Mills, Rev. Sci. Instr. **39** (1968) 105.
12) V.G. Cooper, Appl. Opt. **10** (1971) 525.
13) S. Hess, Physica **61** (1972) 80.
14) P. Harteck and H.W. Schmidt, Z. Phys. Chem. (Leipzig) **B21** (1933) 447.
15) M. Lipsicas, J. Chem. Phys. **36** (1962) 1235.
16) A. Hartland and M. Lipsicas, Phys. Lett. **3** (1962) 212.
17) V.G. Cooper, A.D. May, E.H. Hara and H.F.P. Knaap, Can. J. Phys. **46** (1968) 2019.
18) B.K. Gupta, S. Hess and A.D. May, Can. J. Phys. **50** (1972) 778.
19) K.D. van den Hout, P.W. Hermans and H.F.P. Knaap, Physica **104A** (1980) 548.
20) K.S. Jammu, G.E. St. John and H.L. Welsh, Can. J. Phys. **44** (1966) 797.
21) V.G. Cooper, A.D. May and B.K. Gupta, Can. J. Phys. **48** (1970) 725.
22) R. Shafer and R.G. Gordon, J. Chem. Phys. **58** (1973) 5422.
23) P.W. Anderson, Phys. Rev. **76** (1949) 647.
24) A. Ben-Reuven, Phys. Rev. **145** (1966) 7.
25) J.O. Hirschfelder, C.F. Curtiss and R.B. Bird, Molecular Theory of Gases and Liquids (Wiley, New York, 1954).
26) C.G. Gray and J. van Kranendonk, Can. J. Phys. **44** (1966) 2411.
27) R. Ramaswamy, H. Rabitz and S. Green, J. Chem. Phys. **66** (1977) 3021.
28) T. Witkowicz and A.D. May, Can. J. Phys. **54** (1976) 575.
29) W.E. Köhler, Z. Naturforsch. **26a** (1971) 1926.
30) K. Takayanagi, Suppl. Prog. Theor. Phys. **25** (1963) 1; Institute of Space and Aeronautical Science, University of Tokyo, Report no. **467** (1971) 229.
31) L.S. Rodberg and L.M. Thaler, Introduction to the Quantum Theory of Scattering (Academic Press, New York, 1967).
32) H. Moraal, Physica **73** (1974) 379.
33) D.A. Coombe and W.E. Köhler, Physica **100A** (1980) 472.
34) R.F. Snider, Physica **78** (1974) 387.
35) G.J. Prangsma, L.J.M. Borsboom, H.F.P. Knaap, C.J.N. van den Meijdenberg and J.J.M. Beenakker, Physica **61** (1972) 527.
36) C.G. Sluyter, H.F.P. Knaap and J.J.M. Beenakker, Physica **30** (1964) 745.
37) W.K. Liu and F.R. McCourt, Chem. Phys. **19** (1977) 137.
38) G.J. Prangsma, J.P.J. Heemskerk, H.F.P. Knaap and J.J.M. Beenakker, Physica **50** (1970) 433.